



(12) **United States Patent**
Shalhon Livne et al.

(10) **Patent No.:** **US 12,387,325 B2**
(45) **Date of Patent:** **Aug. 12, 2025**

(54) **SYSTEM AND METHOD FOR
MACHINE-LEARNING BASED SENSOR
ANALYSIS AND VASCULAR TREE
SEGMENTATION**

(71) Applicant: **Cathworks Ltd.**, Kfar Saba (IL)

(72) Inventors: **Moran Shalhon Livne**, Rosh HaAyin
(IL); **Avishai Baruch Yaari**,
Hod-HaSharon (IL); **Hila Blecher**
Segev, Ramat Ishai (IL); **Tomer**
Shapira, Ra'anana (IL); **Ori Ahron**
Noked Partouche, Ramat Gan (IL)

(73) Assignee: **Cath Works Ltd.**, Kfar Saba (IL)

(*) Notice: Subject to any disclaimer, the term of this
patent is extended or adjusted under 35
U.S.C. 154(b) by 365 days.

(21) Appl. No.: **18/167,022**

(22) Filed: **Feb. 9, 2023**

(65) **Prior Publication Data**

US 2023/0252632 A1 Aug. 10, 2023

Related U.S. Application Data

(60) Provisional application No. 63/308,550, filed on Feb.
10, 2022.

(51) **Int. Cl.**
G06V 10/764 (2022.01)
G06T 7/00 (2017.01)
(Continued)

(52) **U.S. Cl.**
CPC **G06T 7/0012** (2013.01); **G06T 7/0016**
(2013.01); **G06T 7/11** (2017.01);
(Continued)

(58) **Field of Classification Search**

None
See application file for complete search history.

(56) **References Cited**

U.S. PATENT DOCUMENTS

5,150,292 A 9/1992 Hoffmann et al.
5,638,823 A 6/1997 Akay et al.
(Continued)

FOREIGN PATENT DOCUMENTS

AU 2010298333 1/2012
CN 104282009 1/2015
(Continued)

OTHER PUBLICATIONS

Abraham et al., "Alternative routes in road networks", ACM Journal
of Experimental Algorithmics, Association of Computing Machin-
ery, vol. 18(1):1.3:2-1.3:17 (2013).

(Continued)

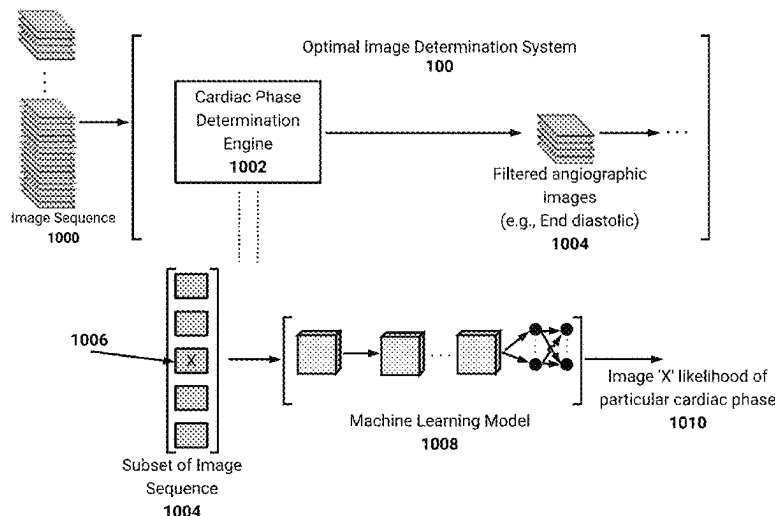
Primary Examiner — Tsung Yin Tsai

(74) *Attorney, Agent, or Firm* — Knobbe, Martens, Olson
& Bear, LLP

(57) **ABSTRACT**

Methods for automated identification of vascular features
are described. In some embodiments, one or more machine
learning (ML)-based vascular classifiers are used, with their
results being combined to with results of at least one other
vascular classifier in order to produce the final results.
Potentially advantages of this approach include the ability to
combine certain strengths of ML classifiers with segmenta-
tion approaches based on more classical ("formula-based")
methods. These strengths may include particularly the iden-
tification of anatomically identified targets mixed within an
image also showing similar looking but anatomically dis-
tinct targets.

20 Claims, 15 Drawing Sheets



- (51) **Int. Cl.**
G06T 7/11 (2017.01)
G06T 7/33 (2017.01)
G06T 7/62 (2017.01)
- (52) **U.S. Cl.**
CPC **G06T 7/33** (2017.01); **G06T 7/62**
(2017.01); **G06V 10/764** (2022.01); **G06T**
2207/20081 (2013.01); **G06T 2207/20084**
(2013.01); **G06T 2207/30048** (2013.01); **G06T**
2207/30101 (2013.01); **G06T 2207/30168**
(2013.01)
- (56) **References Cited**
U.S. PATENT DOCUMENTS
- | | | | |
|------------|------|---------|------------------------------------|
| 6,047,080 | A | 4/2000 | Chen et al. |
| 6,186,948 | B1 | 2/2001 | Kamiyama et al. |
| 6,236,878 | B1 | 5/2001 | Taylor et al. |
| 6,501,848 | B1 | 12/2002 | Carroll et al. |
| 6,842,638 | B1 | 1/2005 | Suri et al. |
| 7,113,623 | B2 | 9/2006 | Chen et al. |
| 7,339,585 | B2 | 3/2008 | Verstraelen et al. |
| 7,369,691 | B2 | 5/2008 | Kondo et al. |
| 7,574,026 | B2 | 8/2009 | Rasche et al. |
| 7,657,299 | B2 | 2/2010 | Huizenga et al. |
| 7,693,315 | B2 | 4/2010 | Krishnan et al. |
| 7,738,626 | B2 | 6/2010 | Weese et al. |
| 7,808,503 | B2 | 10/2010 | Duluk, Jr. et al. |
| 7,860,283 | B2 | 12/2010 | Begelman et al. |
| 7,864,997 | B2 | 1/2011 | Aben |
| 7,912,260 | B2 | 3/2011 | Breeuwer et al. |
| 7,970,187 | B2 | 6/2011 | Puts et al. |
| 7,983,459 | B2 | 7/2011 | Begelman et al. |
| 8,073,224 | B2 | 12/2011 | Strobel et al. |
| 8,086,000 | B2 | 12/2011 | Weijers et al. |
| 8,090,164 | B2 | 1/2012 | Bullitt et al. |
| 8,155,411 | B2 | 4/2012 | Hof et al. |
| 8,298,147 | B2 | 10/2012 | Huennekens et al. |
| 8,311,748 | B2 | 11/2012 | Taylor et al. |
| 8,311,750 | B2 | 11/2012 | Taylor |
| 8,315,812 | B2 | 11/2012 | Taylor |
| 8,321,150 | B2 | 11/2012 | Taylor |
| 8,331,314 | B2 | 12/2012 | Quiang et al. |
| 8,496,594 | B2 | 7/2013 | Taylor et al. |
| 8,523,779 | B2 | 9/2013 | Taylor et al. |
| 8,548,778 | B1 | 10/2013 | Hart et al. |
| 8,554,490 | B2 | 10/2013 | Tang et al. |
| 8,560,968 | B1 | 10/2013 | Nair |
| 8,715,184 | B2 | 5/2014 | Lazebnik |
| 8,768,669 | B1 | 7/2014 | Hart et al. |
| 8,771,195 | B2 | 7/2014 | Kim et al. |
| 8,787,641 | B2 | 7/2014 | Hof et al. |
| 8,812,246 | B2 | 8/2014 | Taylor |
| 8,824,752 | B1 | 9/2014 | Fonte et al. |
| 8,837,860 | B1 | 9/2014 | Grady et al. |
| 8,861,820 | B2 | 10/2014 | Fonte et al. |
| 8,917,925 | B1 | 12/2014 | Grady et al. |
| 8,934,686 | B2 | 1/2015 | Ostrovsky-Berman et al. |
| 8,970,578 | B2 | 3/2015 | Voros et al. |
| 9,008,405 | B2 | 4/2015 | Fonte et al. |
| 9,042,611 | B2 * | 5/2015 | Blezek G06V 20/64
382/128 |
| 9,042,613 | B2 | 5/2015 | Spilker et al. |
| 9,070,214 | B1 | 6/2015 | Grady et al. |
| 9,078,564 | B2 | 7/2015 | Taylor |
| 9,087,147 | B1 | 7/2015 | Fonte |
| 9,129,418 | B2 | 9/2015 | Schormans et al. |
| 9,138,147 | B2 | 9/2015 | Schmitt et al. |
| 9,153,047 | B1 | 10/2015 | Grady et al. |
| 9,189,600 | B2 | 11/2015 | Spilker et al. |
| 9,256,936 | B2 | 2/2016 | Jacobs et al. |
| 9,314,584 | B1 | 4/2016 | Riley et al. |
| 9,375,191 | B2 | 6/2016 | Verstraelen et al. |
| 9,406,141 | B2 | 8/2016 | Kelm et al. |
| 9,430,827 | B2 | 8/2016 | Kelm et al. |
| 9,466,117 | B2 | 10/2016 | Habets et al. |
| 9,471,999 | B2 | 10/2016 | Ishii et al. |
| 9,572,495 | B2 | 2/2017 | Schmitt et al. |
| 9,576,360 | B2 | 2/2017 | Schormans et al. |
| 9,613,186 | B2 | 4/2017 | Fonte |
| 9,615,755 | B2 | 4/2017 | Riley et al. |
| 9,633,454 | B2 | 4/2017 | Lauritsch et al. |
| 9,646,361 | B2 | 5/2017 | Koo et al. |
| 9,706,925 | B2 | 7/2017 | Taylor |
| 9,743,835 | B2 | 8/2017 | Taylor |
| 9,754,082 | B2 | 9/2017 | Taylor et al. |
| 9,786,068 | B2 | 10/2017 | Ishii et al. |
| 9,801,689 | B2 | 10/2017 | Taylor |
| 9,805,465 | B2 | 10/2017 | Kyriakou |
| 9,814,433 | B2 | 11/2017 | Benishti et al. |
| 9,858,387 | B2 | 1/2018 | Lavi et al. |
| 9,870,634 | B2 | 1/2018 | Grady et al. |
| 9,888,896 | B2 | 2/2018 | Lauritsch et al. |
| 9,934,566 | B2 | 4/2018 | Sun et al. |
| 9,940,736 | B2 | 4/2018 | Ishii et al. |
| 9,943,233 | B2 | 4/2018 | Lavi et al. |
| 9,965,873 | B2 | 5/2018 | Grady et al. |
| 9,968,256 | B2 | 5/2018 | Taokowsky et al. |
| 9,977,869 | B2 | 5/2018 | Lavi et al. |
| 9,999,361 | B2 | 6/2018 | Sharma et al. |
| 10,141,074 | B2 | 11/2018 | Lavi et al. |
| 10,143,390 | B2 | 12/2018 | Ledoux et al. |
| 10,159,529 | B2 | 12/2018 | Taylor |
| 10,176,575 | B2 | 1/2019 | Isgum et al. |
| 10,210,956 | B2 | 2/2019 | Lavi et al. |
| 10,219,704 | B2 | 3/2019 | Lavi et al. |
| 10,229,516 | B2 | 3/2019 | Aben et al. |
| 10,235,796 | B2 | 3/2019 | Aben et al. |
| 10,245,001 | B2 | 4/2019 | Redel et al. |
| 10,342,442 | B2 | 7/2019 | Hattangadi et al. |
| 10,354,744 | B2 | 7/2019 | Sharma et al. |
| 10,360,674 | B2 | 7/2019 | Contini et al. |
| 10,363,018 | B2 | 7/2019 | Fukuda et al. |
| 10,373,700 | B2 | 8/2019 | Sharma et al. |
| 10,376,165 | B2 | 8/2019 | Lavi et al. |
| 10,395,366 | B2 | 8/2019 | Isgum et al. |
| 10,395,774 | B2 | 8/2019 | Lavi et al. |
| 10,420,610 | B2 | 9/2019 | Bai et al. |
| 10,424,063 | B2 | 9/2019 | Lavi et al. |
| 10,441,235 | B2 | 10/2019 | Lavi et al. |
| 10,441,239 | B2 | 10/2019 | Abe |
| 10,456,094 | B2 | 10/2019 | Fonte et al. |
| 10,463,336 | B2 | 11/2019 | Itu et al. |
| 10,470,730 | B2 | 11/2019 | Benishti et al. |
| 10,559,388 | B2 | 2/2020 | Lavi et al. |
| 10,580,141 | B2 | 3/2020 | Freiman et al. |
| 10,580,526 | B2 | 3/2020 | Ma et al. |
| 10,595,807 | B2 | 3/2020 | Lavi et al. |
| 10,631,737 | B2 | 4/2020 | Lavi et al. |
| 10,636,146 | B2 | 4/2020 | Zhong et al. |
| 10,650,522 | B2 | 5/2020 | Hoi et al. |
| 10,682,180 | B2 | 6/2020 | Taylor |
| 10,699,407 | B2 | 6/2020 | Isgum et al. |
| 10,702,339 | B2 | 7/2020 | Taylor |
| 10,733,792 | B2 | 8/2020 | Aben et al. |
| 10,740,961 | B2 | 8/2020 | Reiber et al. |
| 10,748,285 | B2 | 8/2020 | Igarashi et al. |
| 10,758,200 | B2 | 9/2020 | Passerini et al. |
| 10,776,988 | B2 | 9/2020 | Grady et al. |
| 10,803,994 | B2 | 10/2020 | Lavi et al. |
| 10,803,995 | B2 | 10/2020 | Sharma et al. |
| 10,828,109 | B2 | 11/2020 | Redel |
| 10,854,329 | B2 | 12/2020 | Mohr et al. |
| 10,964,017 | B2 | 3/2021 | Pack et al. |
| 10,964,071 | B2 | 3/2021 | Grady et al. |
| 11,004,198 | B2 | 5/2021 | Isgum et al. |
| 11,017,531 | B2 | 5/2021 | Harish et al. |
| 11,031,136 | B2 | 6/2021 | Grass et al. |
| 11,051,779 | B2 | 7/2021 | Turca et al. |
| 11,055,845 | B2 | 7/2021 | Nickisch et al. |
| 11,076,770 | B2 | 8/2021 | Lavi et al. |
| 11,081,237 | B2 | 8/2021 | Lavi et al. |
| 11,083,377 | B2 | 8/2021 | Bouwman et al. |
| 11,083,524 | B2 | 8/2021 | Taylor |
| 11,087,884 | B2 | 8/2021 | Sankaran et al. |

(56)

References Cited

U.S. PATENT DOCUMENTS

11,090,118 B2	8/2021	Taylor	11,678,853 B2	6/2023	Gulsun et al.
11,116,575 B2	9/2021	Taylor	11,678,937 B2	6/2023	Choi et al.
11,127,503 B2	9/2021	Rabbat et al.	11,688,502 B2	6/2023	Anderson et al.
11,138,733 B2	10/2021	Lavi et al.	11,690,518 B2	7/2023	Haase et al.
11,141,123 B2	10/2021	Homann et al.	11,694,339 B2	7/2023	Schormans et al.
11,160,524 B2	11/2021	Lavi et al.	11,707,196 B2	7/2023	Lavi et al.
11,179,043 B2	11/2021	Haase et al.	11,707,242 B2	7/2023	Van Walsum et al.
11,185,368 B2	11/2021	Spilker et al.	11,710,569 B2	7/2023	Grass et al.
11,195,278 B2	12/2021	Nickisch et al.	11,728,037 B2	8/2023	Lavi et al.
11,202,612 B2	12/2021	Sakaguchi	11,741,574 B2	8/2023	Kweon et al.
11,216,944 B2	1/2022	Reiber et al.	11,741,602 B2	8/2023	Reiber et al.
11,272,845 B2	3/2022	Cheline et al.	11,744,472 B2	9/2023	Zhao et al.
11,278,208 B2	3/2022	Lavi et al.	11,744,544 B2	9/2023	Sheehan et al.
11,282,170 B2	3/2022	Gauriau et al.	11,748,902 B2	9/2023	Bai et al.
11,288,811 B2	3/2022	Tu et al.	11,756,195 B2	9/2023	Kweon et al.
11,288,813 B2	3/2022	Grady et al.	11,769,254 B2	9/2023	Song et al.
11,295,864 B2	4/2022	Benishti et al.	11,776,149 B2	10/2023	Wang et al.
11,298,187 B2	4/2022	Taylor	11,779,225 B2	10/2023	Adiyoso
11,304,665 B2	4/2022	Sharma et al.	11,779,233 B2	10/2023	Huo et al.
11,308,621 B2	4/2022	Tu et al.	11,779,294 B2	10/2023	Liu et al.
11,328,824 B2	5/2022	Fonte	11,786,202 B2	10/2023	Yin et al.
11,341,631 B2	5/2022	Song et al.	11,793,575 B2	10/2023	Taylor
11,375,904 B2	7/2022	Igarashi	11,803,966 B2	10/2023	Denzinger et al.
11,382,569 B2	7/2022	Grady et al.	11,810,290 B2	11/2023	Flohr et al.
11,389,130 B2	7/2022	Itu et al.	11,810,661 B2	11/2023	Barley et al.
11,398,029 B2	7/2022	Grady et al.	11,816,836 B2	11/2023	Isgum et al.
11,406,337 B2	8/2022	Lavi et al.	11,816,837 B2	11/2023	Lavi et al.
11,406,339 B2	8/2022	Mistretta et al.	11,826,106 B2	11/2023	Hart et al.
11,409,422 B2	8/2022	Olivan Bescos et al.	11,826,175 B2	11/2023	Itu et al.
11,410,308 B2	8/2022	Gulsun et al.	11,847,547 B2	12/2023	Wang et al.
11,423,532 B2	8/2022	Takahashi et al.	11,861,825 B2	1/2024	Van Pelt et al.
11,424,036 B2	8/2022	Fonte et al.	11,861,839 B2	1/2024	Weese et al.
11,424,038 B2	8/2022	Grady et al.	11,861,851 B2	1/2024	Figueroa-Alvarez et al.
11,443,428 B2	9/2022	Petersen et al.	11,869,142 B2	1/2024	Bai et al.
11,445,923 B2	9/2022	Tu et al.	11,883,225 B2	1/2024	Sankaran et al.
11,462,326 B2	10/2022	Wang et al.	11,896,416 B2	2/2024	Huo et al.
11,462,329 B2	10/2022	Rabbat et al.	11,901,081 B2	2/2024	Huo et al.
11,468,567 B2	10/2022	Groth et al.	11,918,291 B2	3/2024	Grass et al.
11,482,339 B2	10/2022	Koo et al.	11,931,195 B2	3/2024	Itu et al.
11,490,867 B2	11/2022	Homann et al.	11,937,963 B2	3/2024	Lavi et al.
11,494,904 B2	11/2022	Fonte et al.	11,944,387 B2	4/2024	Sankaran et al.
11,495,357 B2	11/2022	Ma et al.	11,948,677 B2	4/2024	Ghose et al.
11,501,485 B2	11/2022	Grady et al.	11,948,695 B2	4/2024	Taylor et al.
11,508,460 B2	11/2022	Wang et al.	11,980,492 B2	5/2024	Venugopal et al.
11,510,587 B2	11/2022	Kristanto et al.	11,983,473 B2	5/2024	Aben et al.
11,521,755 B2	12/2022	Taylor et al.	11,986,280 B2	5/2024	Grady et al.
11,523,744 B2	12/2022	Freiman et al.	11,995,834 B2	5/2024	Neumann et al.
11,538,161 B2	12/2022	Wang et al.	12,016,635 B2	6/2024	Taylor
11,540,931 B2	1/2023	Grady et al.	12,023,189 B2	7/2024	Haase et al.
11,557,036 B2	1/2023	Liao et al.	12,027,253 B2	7/2024	Schoebinger et al.
11,557,069 B2	1/2023	Senzig et al.	12,029,494 B2	7/2024	Taylor
11,559,274 B2	1/2023	Auvray et al.	12,039,729 B2	7/2024	Kweon et al.
11,564,746 B2	1/2023	Spilker et al.	12,048,575 B2	7/2024	Vaillant et al.
11,564,748 B2	1/2023	Thienphrapa et al.	12,051,192 B2	7/2024	Aben et al.
11,574,406 B2	2/2023	Chen et al.	12,051,202 B2	7/2024	Freiman et al.
11,576,621 B2	2/2023	Sharma et al.	12,051,497 B2	7/2024	Grady et al.
11,576,626 B2	2/2023	Fonte et al.	12,062,198 B2	8/2024	Liu et al.
11,576,637 B2	2/2023	Schmitt et al.	12,067,729 B2	8/2024	Thamm et al.
11,576,639 B2	2/2023	Song et al.	12,079,994 B2	9/2024	Lavi et al.
11,583,340 B2	2/2023	Taylor	12,089,977 B2	9/2024	Isgum et al.
11,589,924 B2	2/2023	Passerini et al.	12,094,112 B2	9/2024	Gulsun et al.
11,599,996 B2	3/2023	Isgum et al.	12,094,188 B2	9/2024	Li et al.
11,607,189 B2	3/2023	Tu et al.	12,094,596 B2	9/2024	Wang et al.
11,610,309 B2	3/2023	Kweon et al.	12,100,174 B2	9/2024	Vaillant et al.
11,610,318 B2	3/2023	Grady et al.	12,100,502 B2	9/2024	Cimen et al.
11,615,529 B2	3/2023	Chitiboi	12,109,061 B2	10/2024	Itu et al.
11,615,894 B2	3/2023	Lavi et al.	12,109,065 B2	10/2024	Sheehan et al.
11,617,620 B2	4/2023	Tran et al.	12,112,471 B2	10/2024	Viti et al.
11,633,118 B2	4/2023	Freiman et al.	12,112,483 B2	10/2024	Grady et al.
11,638,609 B2	5/2023	Sankaran et al.	12,115,014 B2	10/2024	Haase et al.
11,642,171 B2	5/2023	Jaquet et al.	12,118,724 B2	10/2024	Van Pelt et al.
11,653,833 B2	5/2023	Sanders et al.	12,119,117 B2	10/2024	Wang et al.
11,664,128 B2	5/2023	Haase et al.	12,125,217 B2	10/2024	Venugopal et al.
11,666,236 B2	6/2023	Lavi et al.	12,125,261 B2	10/2024	Petersen et al.
11,672,434 B2	6/2023	Tochterman et al.	12,131,525 B2	10/2024	Groth et al.
			12,136,209 B2	11/2024	Haase et al.
			12,138,026 B2	11/2024	Grady et al.
			12,138,027 B2	11/2024	Lavi et al.
			12,142,384 B2	11/2024	Rabbat et al.

(56)	References Cited		2014/0270442	A1 *	9/2014	Jung	A61B 5/026 382/131
	U.S. PATENT DOCUMENTS		2014/0303495	A1	10/2014	Fonte et al.	
			2014/0371578	A1	12/2014	Auvray et al.	
12,175,631	B2	12/2024	2015/0201897	A1	7/2015	Kyriakou	
12,175,669	B2	12/2024	2015/0213600	A1	7/2015	Kyriakou	
12,176,094	B2	12/2024	2015/0250395	A1	9/2015	Igarashi	
12,178,557	B2	12/2024	2015/0265162	A1	9/2015	Lavi et al.	
2003/0105401	A1	6/2003	2015/0265222	A1	9/2015	Sakaguchi	
2004/0019264	A1	1/2004	2015/0297373	A1	10/2015	Schmitt et al.	
2004/0066958	A1	4/2004	2015/0302578	A1	10/2015	Grady et al.	
2005/0041842	A1	2/2005	2015/0335304	A1	11/2015	Lavi et al.	
2005/0043614	A1	2/2005	2015/0339847	A1	11/2015	Benishti et al.	
2005/0249327	A1	11/2005	2015/0342551	A1	12/2015	Lavi et al.	
2005/0272992	A1	12/2005	2016/0007945	A1	1/2016	Taylor	
2006/0036167	A1	2/2006	2016/0015349	A1	1/2016	Ohuchi et al.	
2006/0074285	A1	4/2006	2016/0022371	A1	1/2016	Sauer et al.	
2006/0084862	A1	4/2006	2016/0035088	A1	2/2016	Abramoff et al.	
2007/0031019	A1	2/2007	2016/0035103	A1 *	2/2016	Stawiaski	G06T 7/11 382/130
2007/0167833	A1	7/2007	2016/0073928	A1	3/2016	Soper et al.	
2008/0020362	A1	1/2008	2016/0110866	A1	4/2016	Taylor	
2008/0187199	A1	8/2008	2016/0110867	A1	4/2016	Taylor	
2008/0205722	A1	8/2008	2016/0128661	A1	5/2016	Taylor	
2009/0016483	A1	1/2009	2016/0157802	A1	6/2016	Anderson	
2009/0016587	A1	1/2009	2016/0228000	A1	8/2016	Spaide	
2009/0171321	A1	7/2009	2016/0247279	A1	8/2016	Lavi et al.	
2009/0299640	A1	12/2009	2016/0371456	A1	12/2016	Taylor et al.	
2009/0312648	A1	12/2009	2017/0018116	A1	1/2017	Sun et al.	
2010/0010428	A1	1/2010	2017/0039736	A1	2/2017	Aben et al.	
2010/0017171	A1	1/2010	2017/0224418	A1	8/2017	Boettner et al.	
2010/0021025	A1	1/2010	2017/0286628	A1	10/2017	Shim	
2010/0067760	A1	3/2010	2017/0325770	A1	11/2017	Edic et al.	
2010/0125197	A1	5/2010	2018/0032653	A1	2/2018	Aben et al.	
2010/0160764	A1	6/2010	2018/0075221	A1	3/2018	Vergaro et al.	
2010/0160773	A1	6/2010	2018/0089829	A1	3/2018	Zhong et al.	
2010/0220917	A1	9/2010	2018/0102189	A1	4/2018	Hosoi et al.	
2010/0296709	A1	11/2010	2018/0182096	A1	6/2018	Grady et al.	
2010/0298719	A1	11/2010	2018/0211386	A1	7/2018	Ma et al.	
2011/0015530	A1	1/2011	2018/0235561	A1	8/2018	Lavi et al.	
2011/0096907	A1	4/2011	2018/0243033	A1	8/2018	Tran et al.	
2011/0134433	A1	6/2011	2018/0268941	A1	9/2018	Lavi et al.	
2011/0135175	A1	6/2011	2018/0271614	A1	9/2018	Kunio	
2011/0142313	A1	6/2011	2018/0280088	A1	10/2018	Davies	
2011/0182492	A1	7/2011	2018/0315193	A1	11/2018	Paschalakis et al.	
2012/0014574	A1	1/2012	2018/0330507	A1	11/2018	Schormans et al.	
2012/0041318	A1	2/2012	2018/0344173	A1	12/2018	Tu et al.	
2012/0041739	A1	2/2012	2018/0344174	A9	12/2018	Schmitt et al.	
2012/0053918	A1	3/2012	2019/0005737	A1	1/2019	Auvray et al.	
2012/0053919	A1	3/2012	2019/0019347	A1	1/2019	Auvray et al.	
2012/0053921	A1	3/2012	2019/0130578	A1	5/2019	Gulsun et al.	
2012/0059246	A1	3/2012	2019/0156159	A1	5/2019	Kopparapu	
2012/0059249	A1	3/2012	2019/0172205	A1 *	6/2019	Mao	G06T 7/0014
2012/0062841	A1	3/2012	2019/0180880	A1	6/2019	Lavi et al.	
2012/0072190	A1	3/2012	2019/0282199	A1	9/2019	Merritt	
2012/0075284	A1	3/2012	2019/0380593	A1	12/2019	Bouwman et al.	
2012/0150048	A1	6/2012	2020/0126229	A1	4/2020	Lavi et al.	
2012/0177275	A1	7/2012	2020/0138521	A1	5/2020	Aben et al.	
2012/0230565	A1	9/2012	2020/0160509	A1	5/2020	Pack et al.	
2012/0236032	A1	9/2012	2020/0222018	A1	7/2020	van Walsum et al.	
2012/0243761	A1	9/2012	2020/0226422	A1	7/2020	Li et al.	
2013/0054214	A1	2/2013	2020/0265958	A1	8/2020	Haase et al.	
2013/0060133	A1	3/2013	2020/0337664	A1	10/2020	Homann et al.	
2013/0094745	A1	4/2013	2020/0349708	A1	11/2020	Igarashi et al.	
2013/0158476	A1	6/2013	2020/0394795	A1	12/2020	Isgum et al.	
2013/0182936	A1	7/2013	2021/0022617	A1	1/2021	Zhao et al.	
2013/0226003	A1	8/2013	2021/0035290	A1	2/2021	Aben et al.	
2013/0229621	A1	9/2013	2021/0085397	A1	3/2021	Passerini et al.	
2013/0324842	A1	12/2013	2021/0209757	A1	7/2021	Min et al.	
2014/0005535	A1	1/2014	2021/0244293	A1	8/2021	Belleville	
2014/0046642	A1	2/2014	2021/0244475	A1	8/2021	Taylor	
2014/0086461	A1	3/2014	2021/0259559	A1	8/2021	Tu et al.	
2014/0094693	A1	4/2014	2021/0267690	A1	9/2021	Taylor	
2014/0094697	A1	4/2014	2021/0272030	A1	9/2021	Sankaran et al.	
2014/0100451	A1	4/2014	2021/0275124	A1	9/2021	Huo et al.	
2014/0121513	A1	5/2014	2021/0280318	A1	9/2021	Huo et al.	
2014/0142398	A1	5/2014	2021/0282731	A1	9/2021	Vaillant et al.	
2014/0200867	A1	7/2014	2021/0282860	A1	9/2021	Taylor	
2014/0249790	A1	9/2014	2021/0290308	A1	9/2021	Mihalef et al.	

(56)

References Cited

U.S. PATENT DOCUMENTS

2021/0298706	A1	9/2021	Tu et al.	2023/0142219	A1	5/2023	Makino
2021/0298708	A1	9/2021	Aben et al.	2023/0144624	A1	5/2023	Venugopal et al.
2021/0334963	A1	10/2021	Isgum et al.	2023/0144795	A1	5/2023	Wang et al.
2021/0338088	A1	11/2021	Bouwman et al.	2023/0148977	A1	5/2023	Fonte et al.
2021/0345889	A1	11/2021	Tu et al.	2023/0177677	A1	6/2023	Yuan et al.
2021/0358634	A1	11/2021	Sankaran et al.	2023/0186472	A1	6/2023	Kweon et al.
2021/0361174	A1	11/2021	Lavi et al.	2023/0196582	A1	6/2023	Grady et al.
2021/0361176	A1	11/2021	Huo et al.	2023/0197286	A1	6/2023	Grady et al.
2021/0374950	A1	12/2021	Gao et al.	2023/0230235	A1	7/2023	Isgum et al.
2021/0375474	A1	12/2021	Lavi et al.	2023/0237648	A1	7/2023	Gulsun et al.
2021/0383539	A1	12/2021	Haase et al.	2023/0237652	A1	7/2023	Flexman et al.
2021/0401400	A1	12/2021	Sheehan et al.	2023/0245301	A1	8/2023	Wang et al.
2022/0012876	A1	1/2022	Sommer et al.	2023/0252628	A1	8/2023	Haase et al.
2022/0012878	A1	1/2022	Aoyama	2023/0263401	A1	8/2023	Escaned-Barbosa et al.
2022/0015730	A1	1/2022	Haase et al.	2023/0277247	A1	9/2023	Taylor et al.
2022/0028080	A1	1/2022	Lavi et al.	2023/0282365	A1	9/2023	Lavi et al.
2022/0036646	A1	2/2022	Song et al.	2023/0298176	A1	9/2023	Choi et al.
2022/0039769	A1	2/2022	M et al.	2023/0298180	A1*	9/2023	Kweon A61B 6/481 382/128
2022/0047236	A1	2/2022	Lavi et al.	2023/0307144	A1	9/2023	He et al.
2022/0054022	A1	2/2022	Van Lavieren	2023/0309943	A1	10/2023	van Walsum et al.
2022/0079455	A1	3/2022	Haase et al.	2023/0320789	A1	10/2023	Bai et al.
2022/0079540	A1	3/2022	Sankaran et al.	2023/0326127	A1	10/2023	Zhong et al.
2022/0079563	A1	3/2022	Kemp	2023/0334659	A1	10/2023	Kuo et al.
2022/0087544	A1	3/2022	Schmitt et al.	2023/0346236	A1	11/2023	Lavi et al.
2022/0092775	A1	3/2022	Denzinger et al.	2023/0352152	A1	11/2023	Grady et al.
2022/0092784	A1	3/2022	Tu et al.	2023/0355107	A1	11/2023	Haase et al.
2022/0101535	A1	3/2022	Thamm et al.	2023/0355196	A1	11/2023	Kang et al.
2022/0110687	A1	4/2022	Spilker et al.	2023/0355197	A1	11/2023	Florent et al.
2022/0125398	A1	4/2022	Aben	2023/0360803	A1	11/2023	Sankaran et al.
2022/0151580	A1	5/2022	Itu et al.	2023/0368378	A1	11/2023	Kim et al.
2022/0156918	A1	5/2022	Chitiboi et al.	2023/0386037	A1	11/2023	Denzinger et al.
2022/0164950	A1	5/2022	Aben et al.	2023/0394654	A1	12/2023	Hampe et al.
2022/0164953	A1	5/2022	Gulsun et al.	2023/0404525	A1	12/2023	Sheehan et al.
2022/0167938	A1	6/2022	Grass et al.	2023/0410307	A1	12/2023	Nickisch et al.
2022/0172368	A1	6/2022	Lavi et al.	2024/0029529	A1	1/2024	Scalisi
2022/0183655	A1	6/2022	Huang et al.	2024/0029868	A1	1/2024	Gulsun et al.
2022/0211280	A1	7/2022	Lavi et al.	2024/0046465	A1	2/2024	Sharma et al.
2022/0211439	A1	7/2022	Sankaran et al.	2024/0047043	A1	2/2024	Flexman et al.
2022/0215534	A1	7/2022	Bai et al.	2024/0050159	A1	2/2024	Hart et al.
2022/0230312	A1	7/2022	Choi et al.	2024/0065772	A1	2/2024	Levi et al.
2022/0233081	A1	7/2022	Cheline et al.	2024/0078676	A1	3/2024	Van Pelt et al.
2022/0254028	A1	8/2022	Liu et al.	2024/0096479	A1	3/2024	Kraus et al.
2022/0254131	A1	8/2022	Lavi et al.	2024/0099589	A1	3/2024	Lavi et al.
2022/0261997	A1	8/2022	Liu et al.	2024/0099683	A1	3/2024	Cimen et al.
2022/0262000	A1	8/2022	Haase et al.	2024/0104719	A1	3/2024	Gulsun et al.
2022/0273180	A1	9/2022	Lavi et al.	2024/0126958	A1	4/2024	Aben et al.
2022/0277447	A1	9/2022	Wang et al.	2024/0130674	A1	4/2024	Sonck et al.
2022/0285034	A1	9/2022	Lavi et al.	2024/0130796	A1	4/2024	Song et al.
2022/0287668	A1	9/2022	Gulsun et al.	2024/0153087	A1	5/2024	Lavi et al.
2022/0301156	A1	9/2022	Fang et al.	2024/0164865	A1	5/2024	Kottenstette et al.
2022/0310265	A1	9/2022	Benishti et al.	2024/0169540	A1	5/2024	Bouwman et al.
2022/0319004	A1	10/2022	Bruch-El et al.	2024/0185485	A1	6/2024	Salomon et al.
2022/0319116	A1	10/2022	Wang et al.	2024/0185509	A1	6/2024	Kovler et al.
2022/0335612	A1	10/2022	Bruch-El et al.	2024/0206838	A1	6/2024	Lavi et al.
2022/0344033	A1	10/2022	Wang et al.	2024/0212159	A1	6/2024	Katzmann et al.
2022/0351369	A1	11/2022	Haase et al.	2024/0215937	A1	7/2024	Itu et al.
2022/0359063	A1	11/2022	Tombropoulos et al.	2024/0221355	A1	7/2024	Kweon et al.
2022/0378383	A1	12/2022	Chen et al.	2024/0260919	A1	8/2024	Venugopal et al.
2022/0392616	A1	12/2022	Ghose et al.	2024/0273723	A1	8/2024	Tison et al.
2022/0415510	A1	12/2022	Wang et al.	2024/0315777	A1	9/2024	Choi et al.
2023/0005113	A1	1/2023	Li et al.	2024/0374148	A1	11/2024	Haase et al.
2023/0028300	A1	1/2023	Lichy et al.	2024/0386652	A1	11/2024	Grady et al.
2023/0037338	A1	2/2023	Wang et al.	2024/0394875	A1	11/2024	Van Der Horst et al.
2023/0038364	A1	2/2023	Bhowmick et al.	2024/0394996	A1	11/2024	Hitschrich et al.
2023/0052595	A1	2/2023	Langoju et al.	2024/0404031	A1	12/2024	Auvray et al.
2023/0071558	A1	3/2023	Vaidya et al.	2024/0404057	A1	12/2024	Florent et al.
2023/0084748	A1	3/2023	Lavi et al.	2024/0407656	A1	12/2024	This et al.
2023/0086196	A1	3/2023	Chitiboi et al.	2024/0412365	A1	12/2024	Kim
2023/0095242	A1	3/2023	Liu et al.	2024/0420331	A1	12/2024	Kim et al.
2023/0097133	A1	3/2023	Bai et al.	2024/0423575	A1	12/2024	Itu et al.
2023/0097267	A1	3/2023	Schwemmer et al.	2024/0428477	A1	12/2024	Salehi et al.
2023/0102646	A1	3/2023	Birkhold et al.				
2023/0108647	A1	4/2023	Tu et al.				
2023/0113721	A1	4/2023	Kassel et al.				
2023/0142152	A1	5/2023	Venugopal et al.				

FOREIGN PATENT DOCUMENTS

CN	113837985	12/2021
CN	113935976	1/2022
EP	1396274	3/2004
EP	2163272	3/2010

(56)	References Cited			JP	2003-514600	4/2003
	FOREIGN PATENT DOCUMENTS			JP	2004-243117	9/2004
				JP	2007-502644	2/2007
				JP	2007-325920	12/2007
EP	2633815	A1	9/2013	JP	4177217	B2 11/2008
EP	2779907		9/2014	JP	2010-042247	2/2010
EP	2873371		5/2015	JP	2011-212314	10/2011
EP	3125764		2/2017	JP	2013-090799	5/2013
EP	2633815	B1	6/2017	JP	2010-505493	7/2013
EP	3363350		8/2018	JP	2013-534154	9/2013
EP	2977922		3/2019	JP	2014-064915	4/2014
EP	3460688		3/2019	JP	2014-128631	7/2014
EP	3477551		5/2019	JP	2015-503416	2/2015
EP	3763285		1/2021	JP	2015-527901	9/2015
EP	3847956		7/2021	JP	2016-509501	3/2016
EP	2776960		9/2021	JP	2017-516535	6/2017
EP	3534372		9/2021	JP	2018-057835	4/2018
EP	3871184		9/2021	JP	2018-089364	6/2018
EP	3881758		9/2021	NL	2012324	8/2015
EP	3884868		9/2021	WO	WO 2001/21057	3/2001
EP	3282380		11/2021	WO	WO 2007/066249	6/2007
EP	3282381		11/2021	WO	WO 2010/033971	3/2010
EP	3903672		11/2021	WO	WO 2011/038044	3/2011
EP	3912139		11/2021	WO	WO 2011/039685	4/2011
EP	3664026		2/2022	WO	WO 2012/021037	2/2012
EP	3945469		2/2022	WO	WO 2012/021307	2/2012
EP	3949860		2/2022	WO	WO 2012/043498	4/2012
EP	3951705		2/2022	WO	WO 2012/173697	12/2012
EP	3076854		4/2022	WO	WO 2013/102880	7/2013
EP	3979259		4/2022	WO	WO 2014/027692	2/2014
EP	3982324		4/2022	WO	WO 2014/064702	5/2014
EP	3258446		5/2022	WO	WO 2014/111927	7/2014
EP	4002288		5/2022	WO	WO 2014/111929	7/2014
EP	4026143		7/2022	WO	WO 2014/111930	7/2014
EP	4026491		7/2022	WO	WO 2015/017420	2/2015
EP	4026492		7/2022	WO	WO 2015/059706	4/2015
EP	4029438		7/2022	WO	WO 2016/161356	10/2016
EP	3298959		9/2022	WO	WO 2017/056007	4/2017
EP	3989828		11/2022	WO	WO 2017/199245	11/2017
EP	3157411		12/2022	WO	WO 2017/199246	11/2017
EP	3606437		12/2022	WO	WO 2017/200381	11/2017
EP	4104765		12/2022	WO	WO 2018/165478	9/2018
EP	4113434		1/2023	WO	WO 2018/178272	10/2018
EP	4131150		2/2023	WO	WO 2019/101630	5/2019
EP	4137053		2/2023	WO	WO 2020/053099	3/2020
EP	4145391		3/2023	WO	WO 2020/084101	4/2020
EP	4156112		3/2023	WO	WO 2020/201942	10/2020
EP	3169237		4/2023	WO	WO 2021/016071	1/2021
EP	4160528		4/2023	WO	WO 2021/059165	4/2021
EP	4160543		4/2023	WO	WO 2021/175039	9/2021
EP	4170579		4/2023	WO	WO 2021/191909	9/2021
EP	4186417		5/2023	WO	WO 2021/258835	12/2021
EP	3403582		6/2023	WO	WO 2022/000727	1/2022
EP	3743883		6/2023	WO	WO 2022/000729	1/2022
EP	3989832		8/2023	WO	WO 2022/000733	1/2022
EP	4220553		8/2023	WO	WO 2022/000734	1/2022
EP	4224416		8/2023	WO	WO 2022/000976	1/2022
EP	3652747		9/2023	WO	WO 2022/000977	1/2022
EP	4104766		9/2023	WO	WO 2022/002765	1/2022
EP	4238500		9/2023	WO	WO 2022/019765	1/2022
EP	3602485		10/2023	WO	WO 2022/069208	4/2022
EP	4064181		11/2023	WO	WO 2022/086326	4/2022
EP	3602487		12/2023	WO	WO 2022/109902	6/2022
EP	4300419		1/2024	WO	WO 2022/109903	6/2022
EP	4312184		1/2024	WO	WO 2022/109904	6/2022
EP	3404667		2/2024	WO	WO 2022/109907	6/2022
EP	3878366		4/2024	WO	WO 2022/136043	6/2022
EP	3457413		5/2024	WO	WO 2022/161239	8/2022
EP	4005472		5/2024	WO	WO 2022/167940	8/2022
EP	4369290		5/2024	WO	WO 2022/184736	9/2022
EP	4176814		7/2024	WO	WO 2022/199238	9/2022
EP	4413927		8/2024	WO	WO 2022/235162	11/2022
EP	4418206		8/2024	WO	WO 2022/261641	12/2022
EP	3846176		9/2024	WO	WO 2023/277283	1/2023
EP	3881758	B1	9/2024	WO	WO 2023/057296	4/2023
EP	3564963		10/2024	WO	WO 2023/099144	6/2023
EP	4056110		10/2024	WO	WO 2023/104538	6/2023
JP	H08-131429		5/1996	WO	WO 2023/115576	6/2023
JP	2003-508152		3/2003	WO	WO 2023/146401	8/2023

(56)

References Cited

FOREIGN PATENT DOCUMENTS

WO	WO 2023/152688	8/2023
WO	WO 2023/191380	10/2023
WO	WO 2023/224369	11/2023
WO	WO 2022/228464	12/2023
WO	WO 2024/022809	2/2024
WO	WO 2024/023048	2/2024
WO	WO 2024/034748	2/2024
WO	WO 2024/074309	4/2024
WO	WO 2024/083538	4/2024
WO	WO 2024/121060	6/2024
WO	WO 2024/151926	7/2024
WO	WO 2024/156859	8/2024
WO	WO 2024/160583	8/2024
WO	WO 2024/177428	8/2024

OTHER PUBLICATIONS

Andriotis et al., "A new method of three-dimensional coronary artery reconstruction from X-Ray angiography: Validation against a virtual phantom and multislice computed tomography", *Catheterization and Cardiovascular Interventions*, vol. 71:28-43 (2008).

Barnea, "Model-based estimation of coronary vessel diameter in angiographic images", *Proceedings of the 20th Annual International Conference of the IEEE Engineering in Medicine and Biology Society*, vol. 20:513-516 (1998).

Barratt et al., "Reconstruction and quantification of the carotid artery bifurcation from 3-D ultrasound images", *IEEE Transactions on Medical Imaging*, vol. 23(5):567-583 (2004).

Bullitt et al., "Determining malignancy of brain tumors by analysis of vessel shape", *Medical Image Computing and Computer-Assisted Intervention, MICCAI 2004 Conference Proceedings, Lecture notes in Computer Science, LNCS*, 3217:645-653.

Caiati et al., "New noninvasive method for coronary flow reserve assessment: Contrast-enhanced transthoracic second harmonic echo doppler", *Circulation*, vol. 99:771-778 (1999).

Caiati et al., "Detection, location, and severity assessment of left anterior descending coronary artery stenoses by means of contrast-enhanced transthoracic harmonic echo doppler", *European Heart Journal*, vol. 30:1797-1806 (2009).

Chung, "Image segmentation methods for detecting blood vessels in angiography", *2006 9th International Conference on Control, Automation, Robotics and Vision*, Singapore, pp. 1-6 (2006).

Dickie et al., "Live-vessel: interactive vascular image segmentation with simultaneous extraction of optimal medial and boundary paths", *Technical Report TR 2009-23*, School of Computing Science, Simon Fraser University, Burnaby, BC, Canada, Nov. 2009.

Frangi et al., "Multiscale vessel and enhancement filtering", *Medical Image Computing and Computer-Assisted Intervention, MICCAI '98 Lecture Notes in Computer Science*, vol. 1496:130-137 (1998).

Fraz, "Blood vessel segmentation methodologies, in retinal images—a survey", *Computer Methods and Programs in Biomedicine*, vol. 108:407-433 (2012).

Fusejima, "Noninvasive measurement of coronary artery blood flow using combined two-dimensional and doppler echocardiography", *JACC vol. 10(5):1024-1031* (1987).

Hawkes et al., "Validation of volume blood flow measurements using three-dimensional distance-concentration functions derived from digital X-Ray angiograms", *Investigative Radiology*, vol. 29(4):434-442 (1994).

Hoffmann et al., "Determination of instantaneous and average blood flow rates from digital angiograms of vessel phantoms using distance-density curves", *Investigative Radiology*, vol. 26(3):207-212 (1991).

Holdsworth et al., "Quantitative angiographic blood-flow measurement using pulsed intra-arterial injection", *Medical Physics*, vol. 26(10):2168-2175 (1999).

Huo et al., "Intraspecific scaling laws of vascular trees", *J.R. Soc. Interface* vol. 9:190-200 (2012).

Janssen et al., "New approaches for the assessment of vessel sizes in quantitative (cardio-)vascular X-ray analysis", *Int J Cardiovasc Imaging* vol. 26:259-271 (2010).

Kappetein et al., "Current percutaneous coronary intervention and coronary artery bypass grafting practices for three-vessel and left main coronary artery disease: Insights from the SYNTAX run-in phase", *European Journal of Cardio-Thoracic Surgery*, vol. 29:486-491 (2010).

Kass et al., "Snakes: active contour models", *Int. J. Comput. Vis.* vol. 1:321-331 (1987).

Kirkeeide, "Coronary obstructions, morphology and physiologic significance", *Quantitative Coronary Arteriography*, Chap. 11:229-244 (1991).

Lethen et al., "Validation of noninvasive assessment of coronary flow velocity reserve in the right coronary artery—A comparison of transthoracic echocardiographic results with intracoronary doppler flow wire measurements", *European Heart Journal*, vol. 24:1567-1575 (2003).

Li et al., "Minimization of region-scalable fitting energy for image segmentation", in *IEEE Transactions on Image Processing*, vol. 17(10):1940-1949 (2008).

Meimoun et al., "Non-invasive assessment of coronary flow and coronary flow reserve by transthoracic doppler echocardiography: a magic tool for the real world", *European Journal of Echocardiography*, vol. 9:449-457 (2008).

Mercer-Rosa et al., "Illustration of the additional value of real-time 3-dimensional echocardiography to conventional transthoracic and transesophageal 2-dimensional echocardiography in imaging muscular ventricular septal defects: does this have any impact on individual patient treatment", *Journal of the American Society of Echocardiography*, vol. 19(12):1511-1519 (2006).

Molloi et al., "Quantification of fractional flow reserve using angiographic image data", *World Congress on Medical Physics and Biomedical Engineering*, Munich, Germany, Sep. 7-12, 2009.

Molloi et al., "Estimation of coronary artery hyperemic blood flow based on arterial lumen volume using angiographic images", *Int J Cardiovasc Imaging*, vol. 28:1-11 (2012).

Ng et al., "Novel QCA methodologies and angiographic scores", *Int J Cardiovasc Imaging* vol. 27:157-165 (2011).

Pellot et al., "A 3D reconstruction of vascular structures from two X-Ray angiograms using an adapted simulated annealing algorithm", *IEEE Transactions of Medical Imaging*, vol. 13(1):48-60 (1994).

Pinho et al., "Assessment and stenting of tracheal stenosis using deformable shape models", *Medical Image Analysis*, vol. 15(2):250-266 (2010).

Polytimi et al., "Close to transplant renal artery stenosis and percutaneous transluminal treatment", *Journal of Transplantation*, vol. 2011, 7 pages (2011).

Sarwal et al., "3-D reconstruction of coronary arteries", *Proceedings of the 16th Annual Intl. Conference of the IEEE Engineering in Medicine and Biology Society, Engineering Advances: New Opportunities for Biomedical Engineers*, Nov. 3, 1994, pp. 504-505.

Sato et al., "A viewpoint determination system for stenosis diagnosis and quantification in coronary angiographic image acquisition", *IEEE Transactions on Medical Imaging*, vol. 17(1):121-137 (1998).

Seifalian et al., "A new algorithm for deriving pulsatile blood flow waveforms tested using simulated dynamic angiographic data", *Neuroradiology*, vol. 31:263-269 (1989).

Seifalian et al., "Blood flow measurements using 3D distance-concentration functions derived from digital x-ray angiograms", *Cardiovascular Imaging*, Chap. 33:425-442 (1996).

Seifalian et al., "Validation of a quantitative radiographic technique to estimate pulsatile blood flow waveforms using digital subtraction angiographic data", *Journal of Biomedical Engineering*, vol. 13(3):225-233 (1991).

Shang et al., "Vascular active contour for vessel tree segmentation", in *IEEE Transactions on Biomedical Engineering*, vol. 58(4):1023-1032 (2011).

Shpilfeygel et al., "Comparison of methods for instantaneous angiographic blood flow measurement", *Medical Physics*, vol. 26(6):862-871 (1999).

(56)

References Cited**OTHER PUBLICATIONS**

- Sianos et al., "The SYNTAX score: an angiographic tool grading the complexity of coronary artery disease", *Euro Intervention*, vol. 1(2):219-227 (2005).
- Siogkas et al., "Quantification of the effect of percutaneous coronary angioplasty on a stenosed right coronary artery", 2010 10th IEEE Intl. Conference on Information Technology and Applications in Biomedicine, Nov. 3-5, 210, pp. 1-4 (2010).
- Slomka et al., "Fully automated wall motion and thickening scoring system for myocardial perfusion SPECT: Method development and validation in large population", *Journal of Nuclear Cardiology*, vol. 19(2):291-302 (2012).
- Sprague et al., "Coronary x-ray angiographic reconstruction and image orientation", *Medical Physics*, vol. 33(3):707-718 (2006).
- Sun et al., "Coronary CT angiography: current status and continuing challenges", *The British Journal of Radiology*, vol. 85:495-510 (2012).
- Takarada et al., "An angiographic technique for coronary fractional flow reserve measurement: in vivo validation", *International Journal of Cardiovascular Imaging*, published online pp. 1-10, Aug. 31, 2012.
- Termeer et al., "Visualization of myocardial perfusion derived from coronary anatomy", *IEEE Transactions on Visualization and Computer Graphics*, vol. 14(6):1595-1602 (2008).
- Tomasello et al., "Quantitative coronary angiography in the interventional cardiology", *Advances in the Diagnosis of Coronary Atherosclerosis*, Chap. 14:255-272 (2011).
- Tu et al., "Assessment of obstruction length and optimal viewing angle from biplane X-ray angiograms", *Int J Cardiovasc Imaging*, vol. 26:5-17 (2010).
- Tu et al., "In vivo assessment of optimal viewing angles from X-ray coronary angiography", *EuroIntervention*, vol. 7:112-120 (2011).
- Tu et al., "In vivo assessment of bifurcation optimal viewing angles and bifurcation angles by three-dimensional (3D) quantitative coronary angiography", *Int J Cardiovasc Imaging*, published online Dec. 15, 2011, in 9 pages.
- Tu et al., "The impact of acquisition angle differences on three-dimensional quantitative coronary angiography", *Catheterization and Cardiovascular Interventions*, vol. 78:214-222 (2011).
- Tuinenburg et al., "Dedicated bifurcation analysis: basic principles", *Int J Cardiovasc Imaging*, vol. 27:167-174 (2001).
- Voci et al., "Coronary flow: a new asset for the echo lab?", *European Heart Journal*, vol. 25:1867-1879 (2004).
- Weickert et al., "A scheme for coherence-enhancing diffusion filtering with optimized rotation invariance", *Computer Vision, Graphics, and Pattern Recognition Group, Technical Report, Computer Science Series*, pp. 1-20 (2000).
- Weickert, "Anisotropic diffusion in image processing", ECMI, published by Teubner Stuttgart, Germany, 181 pages (2008).
- Weickert et al., "A scheme for coherence-enhancing diffusion filtering with optimized rotation invariance", *Journal of Visual Communication and Image Representation*, vol. 13(1-2):103-118 (2002).
- Wong et al., "Quantification of fractional flow reserve based on angiographic image data", *The International Journal of Cardiac Imaging*, vol. 28(1):13-22 (2012).
- Wong et al., "Determination of fractional flow reserve (FFR) based on scaling laws: a simulation study", *Physics in Medicine and Biology*, vol. 53:3995-4011 (2008).
- Wong et al., "Automated technique for angiographic determination of coronary blood flow and lumen volume", *Acad. Radiol.* vol. 13:186-194 (2006).
- Xu et al., "Snakes, shapes, and gradient vector flow", *IEEE Transactions on Image Processing*, vol. 7:359-369 (1998).
- Yang et al., "Novel approach for 3-D reconstruction of coronary arteries from two uncalibrated angiographic images", *IEEE Transactions on Image Processing*, vol. 18(7):1563-1572 (2009).
- Rabbat et al., "Interpreting results of coronary computed tomography angiography-derived fractional flow reserve in clinical practice", *Journal of Cardiovascular Computed Tomography*, vol. 11(5):1-6 (2017).
- Extended European Search Report in European Application No. EP 20843503, dated Jul. 7, 2023, in 10 pages.
- International Search Report and Written Opinion in application No. PCT/IB2023/051186, mailed on Jul. 17, 2023, in 15 pages.
- Jiang et al., "Vascular tree reconstruction by minimizing a physiological functional cost", 2010 IEEE Computer Society Conference on Computer Vision and Pattern Recognition—workshops, San Francisco, CA, pp. 178-185, doi: 10.1109/CVPRW.2010.5543593.
- Invitation to Pay Additional Fees in Application No. PCT/IB2023/051186, mailed on May 25, 2023, in 33 pages.
- Hwang et al., "Diagnostic performance of resting and hyperemic invasive physiological indices to define myocardial ischemia", *JACC: Cardiovascular Interventions*, vol. 10(8):751-760 (2017).
- Kern, "Serial lesion FFR made simple", *Cath Lab Digest*, vol. 20(9)(2012), in 2 pages, [retrieved on Sep. 25, 2024], retrieved from the internet: <https://www.hmpgloballearningnetwork.com/site/cathlab/articles/serial-lesion-ffr-made-simple>.
- Neng et al., "Pre-stenting angiography-FFR based physiological map provides virtual intervention and predicts physiological and clinical outcomes", *Catheterization and Cardiovascular Interventions*, Wiley-Liss, New York, NY, vol. 101(6):1053-1061 (2023).
- Nijjer et al., "Pre-angioplasty instantaneous wave-free ratio pullback provides virtual intervention and predicts hemodynamic outcome for serial lesions and diffuse coronary artery disease", *JACC: Cardiovascular Interventions*, vol. 7(12):1386-1396 (2014).
- Pijls et al., "Experimental basis of determining maximum coronary, myocardial, and collateral blood flow by pressure measurements for assessing functional stenosis severity before and after percutaneous transluminal coronary angioplasty", *Circulation*, vol. 87:1354-1367 (1993).
- Rimac et al., "Clinical value of post-percutaneous coronary intervention fractional flow reserve value: A systematic review and meta-analysis", *Am Heart J.* vol. 183:1-9 (2017).
- Volcano Corporation, iFR instant wave-free RatioTM, "An introduction to iFR ScoutTM Pullback Measurements, Moving from Justified PCI to Guided PCI", 2015, in 11 pages, [retrieved on Aug. 29, 2024]. Retrieved from the Internet <URL: <https://www.usa.philips.com/c-dam/b2bhc/master/education-resources/technologies/igt/iFR-Scout-In-Service.pdf>>.
- International Preliminary Report on Patentability and Written Opinion in application No. PCT/IB2023/051186, dated Aug. 6, 2024, in 8 pages.
- Barrett et al., "Interactive live-wire 1-3 boundary extraction", *Medical Image Analysis*, Oxford University Press, vol. 1(4):331-341 (1997).
- Chen et al., "3-D reconstruction of coronary arterial tree to optimize angiographic visualization", *IEEE Transactions on Medical Imaging*, vol. 19(4):318-336 (2000).
- Marchenko, et al., "Vascular editor: from angiographic images to 3D vascular models", *Journal of Digital Imaging*, vol. 23:386-398 (2010).
- Wang et al., "Optimal viewing angle determination for multiple vessel segments in coronary angiographic image", *IEEE Transactions on Nuclear Science*, vol. 61(3):1290-1303 (2014).
- Wang et al., "Global optimization angiographic viewing angles for coronary arteries with multiple segments", 35th Annual International Conference of the IEEE EMBS, pp. 2640-2643, Osaka, Japan, Jul. 3-7, 2013.

* cited by examiner

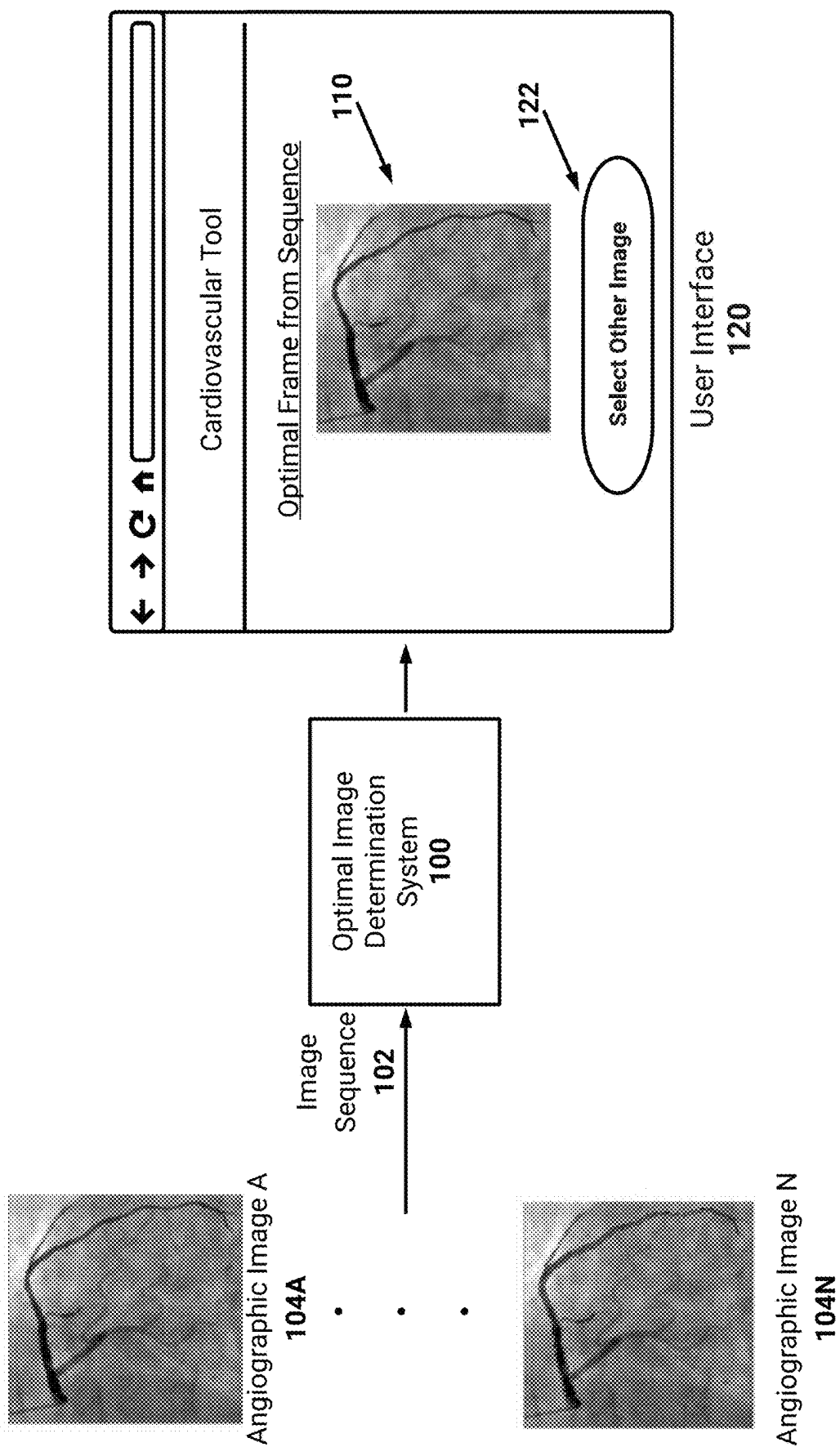
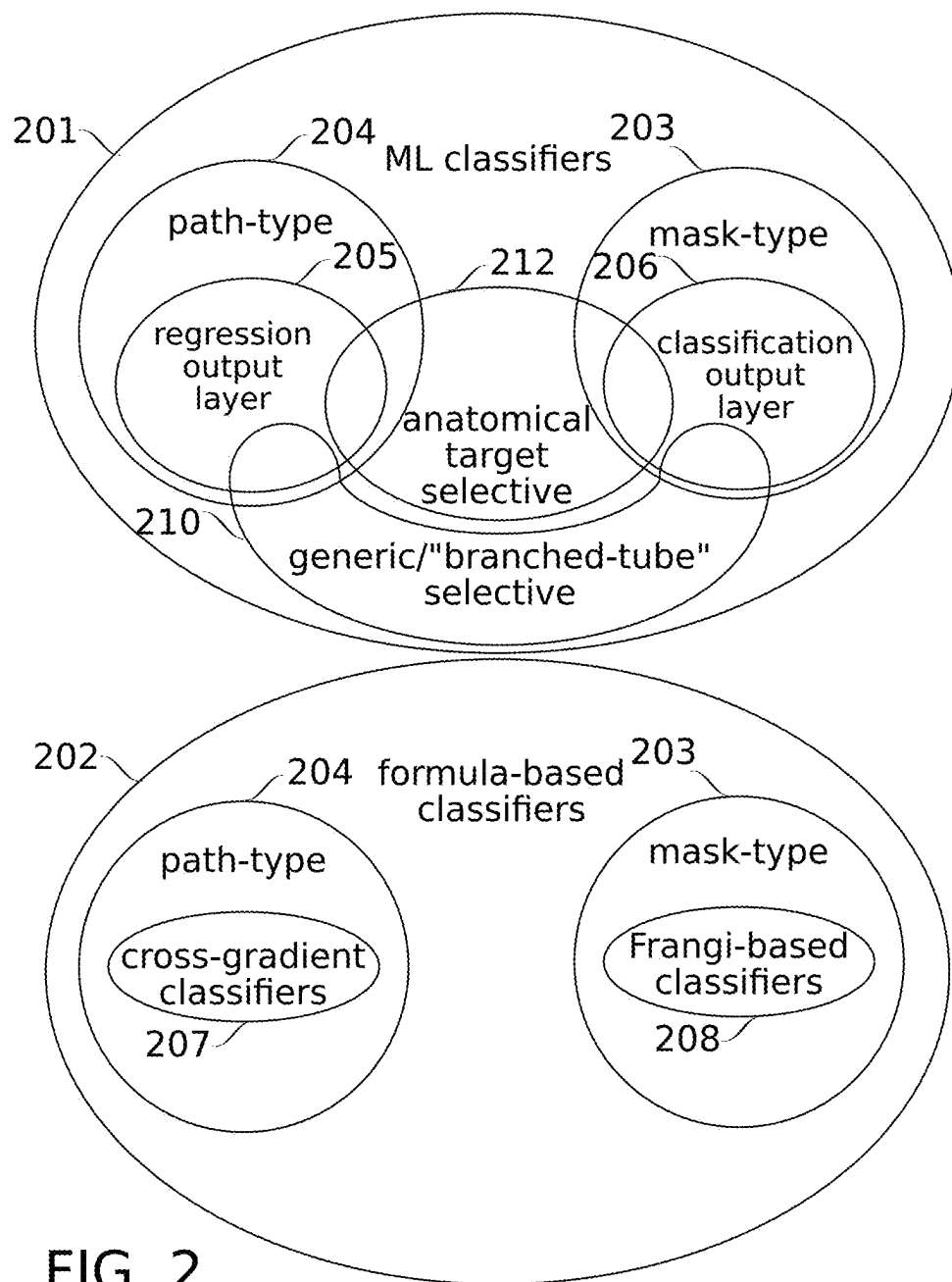


FIG. 1



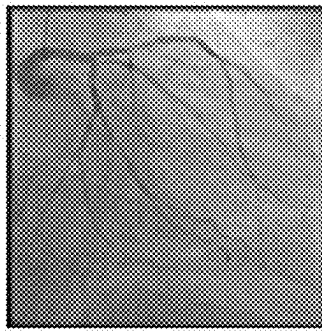


FIG. 3A

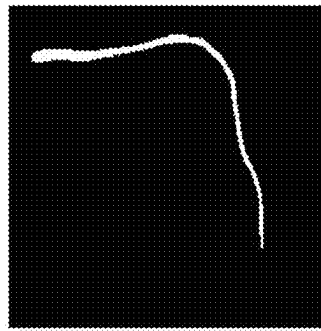


FIG. 3B

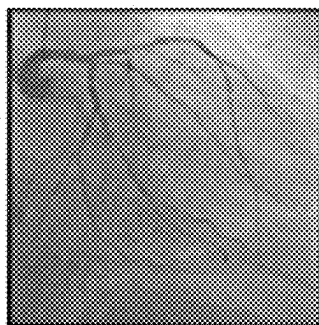


FIG. 3C

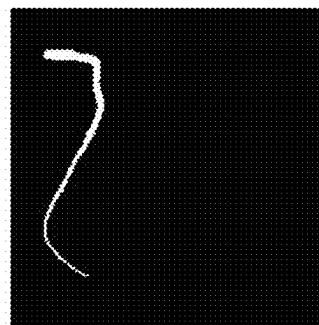


FIG. 3D

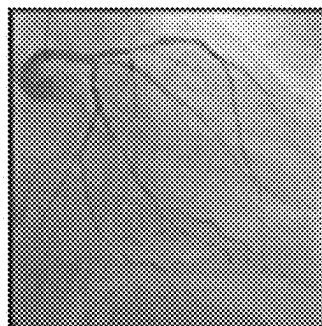


FIG. 3E

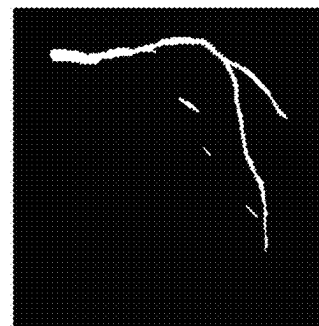


FIG. 3F

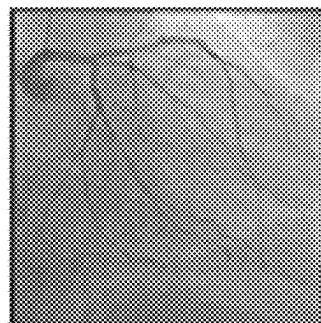


FIG. 3G

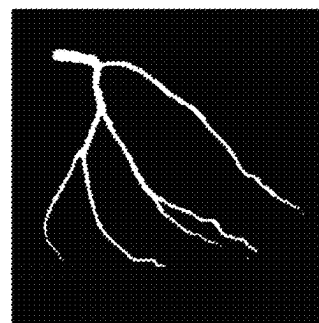


FIG. 3H

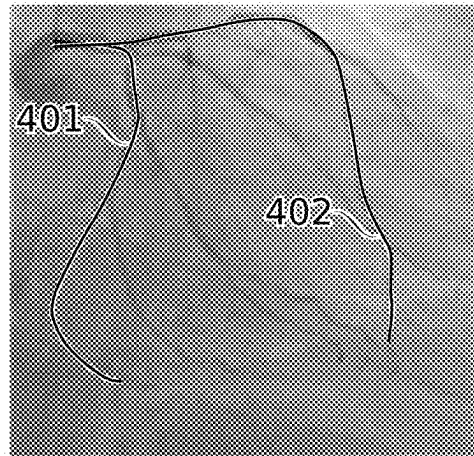


FIG. 4

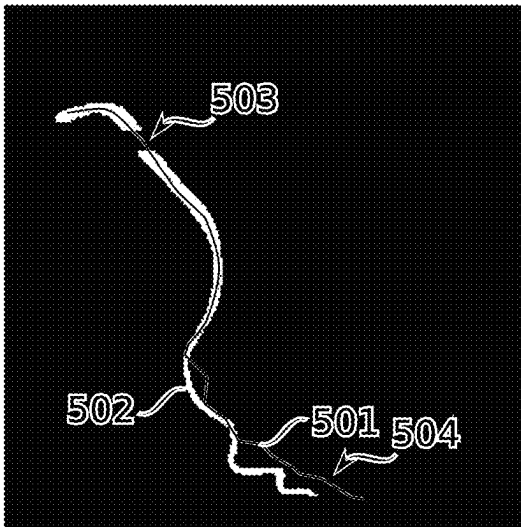


FIG. 5A

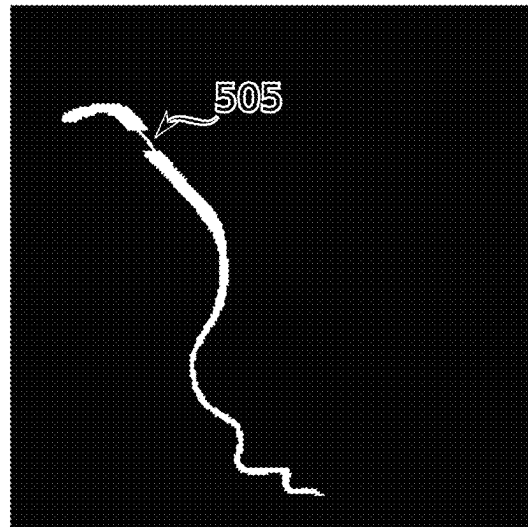


FIG. 5B

FIG. 6A

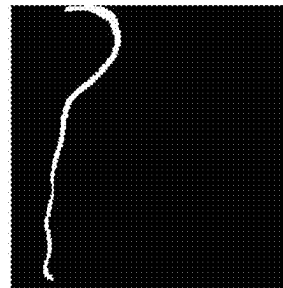
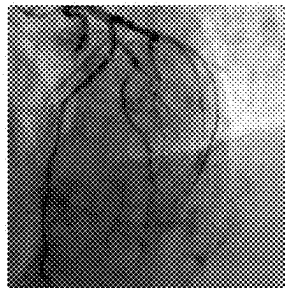


FIG. 6B

FIG. 6C

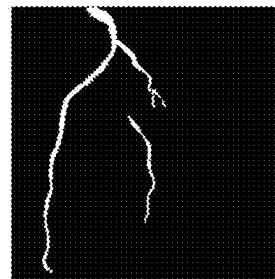
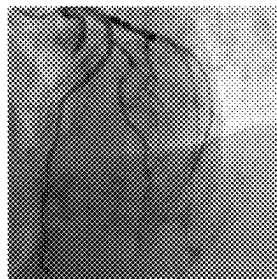


FIG. 6D

FIG. 6E

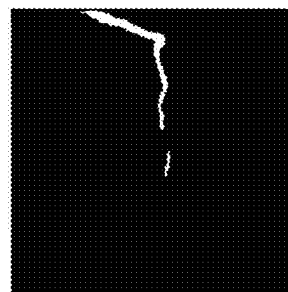
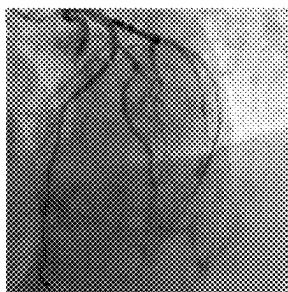


FIG. 6F

FIG. 6G

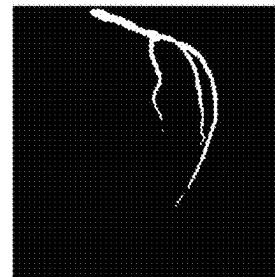
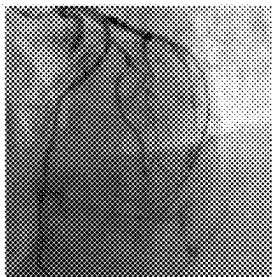


FIG. 6H

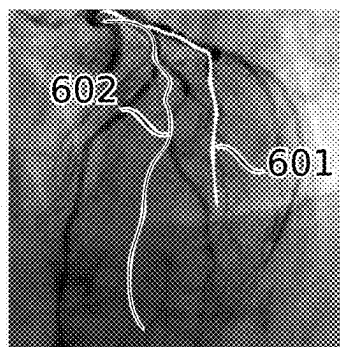


FIG. 6J

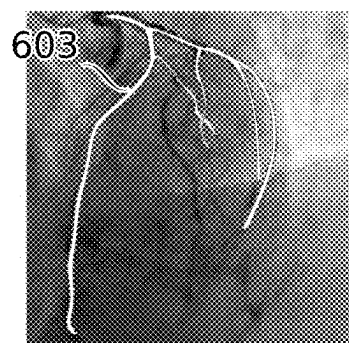


FIG. 6K

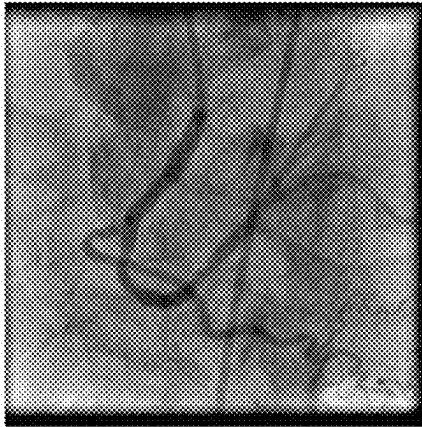


FIG. 7A

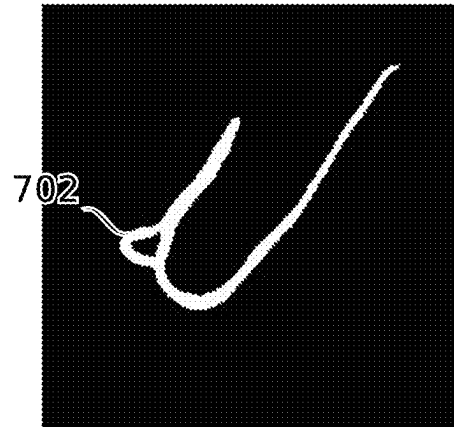


FIG. 7B



FIG. 7C

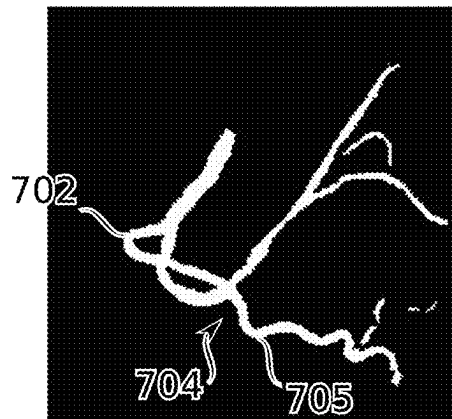


FIG. 7D

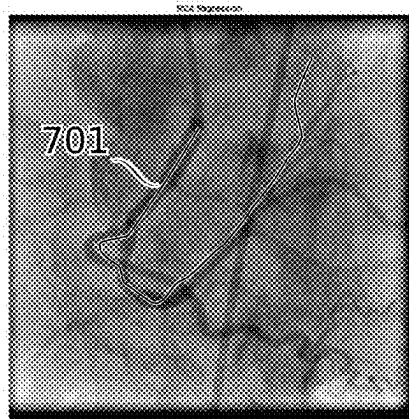


FIG. 7E

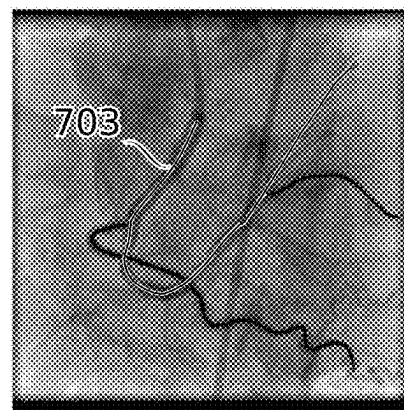


FIG. 7F

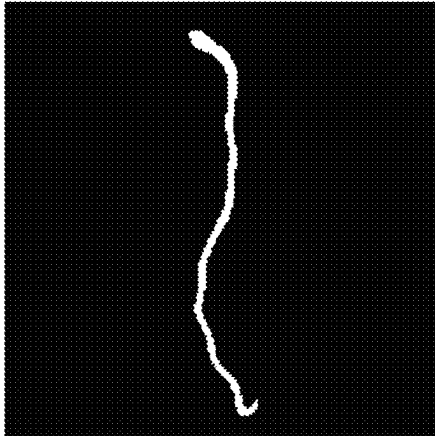


FIG. 8A

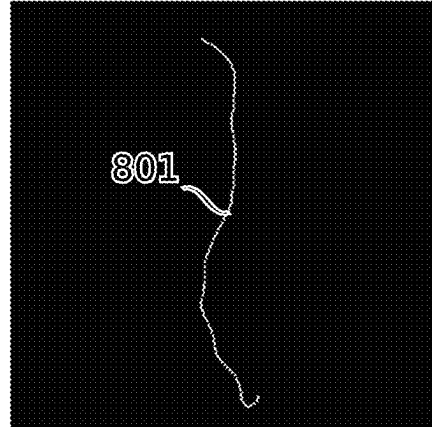


FIG. 8B

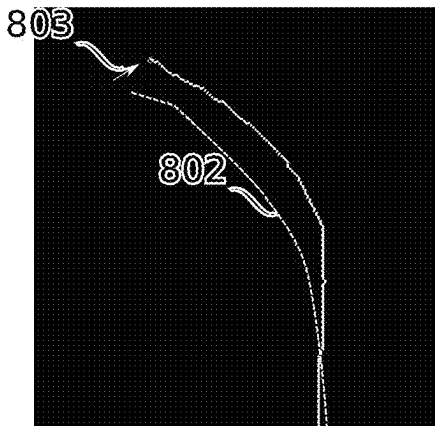


FIG. 8C

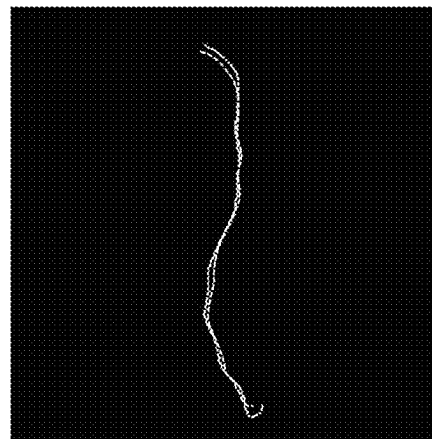


FIG. 8D

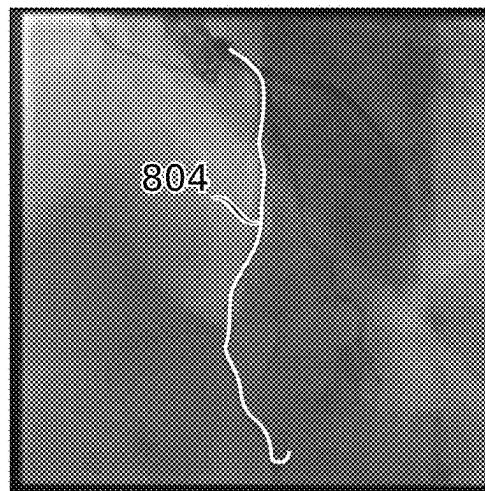


FIG. 8E

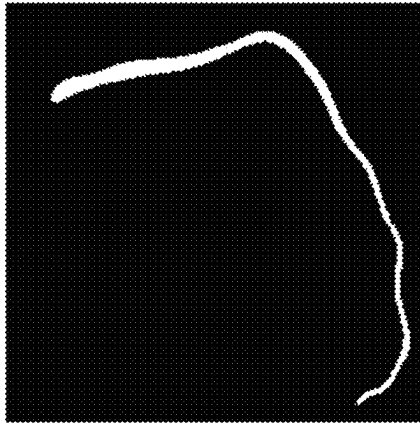


FIG. 9A

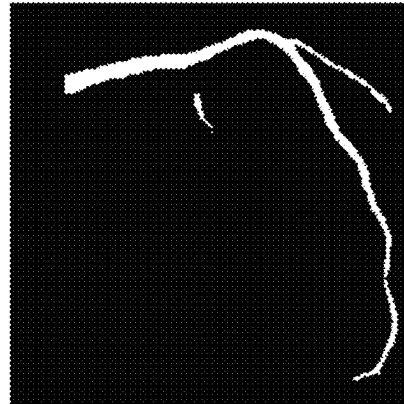


FIG. 9B



FIG. 9C

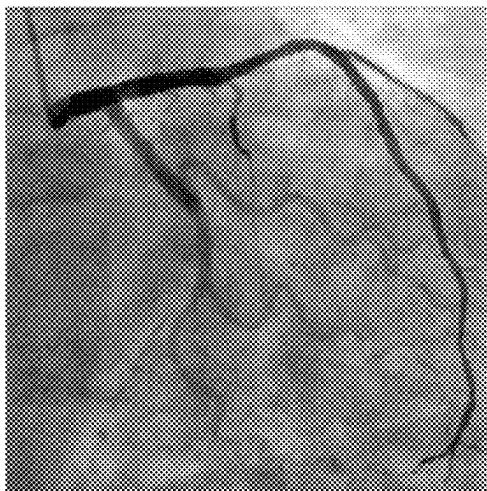


FIG. 9D

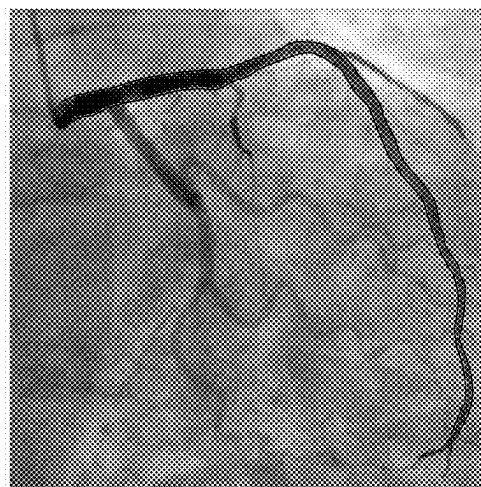


FIG. 9E

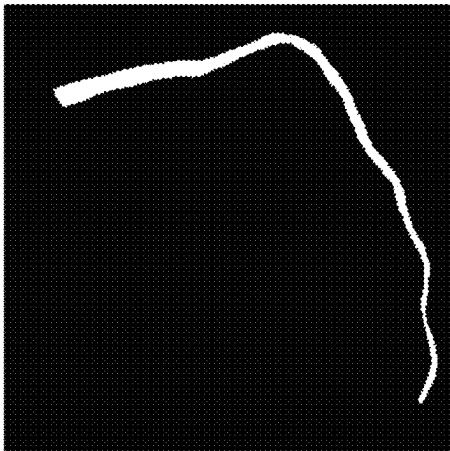


FIG. 9F

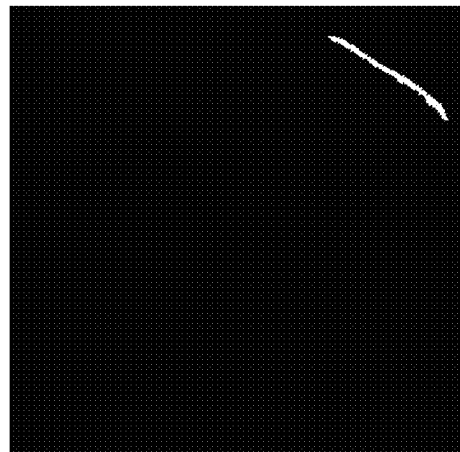


FIG. 9G

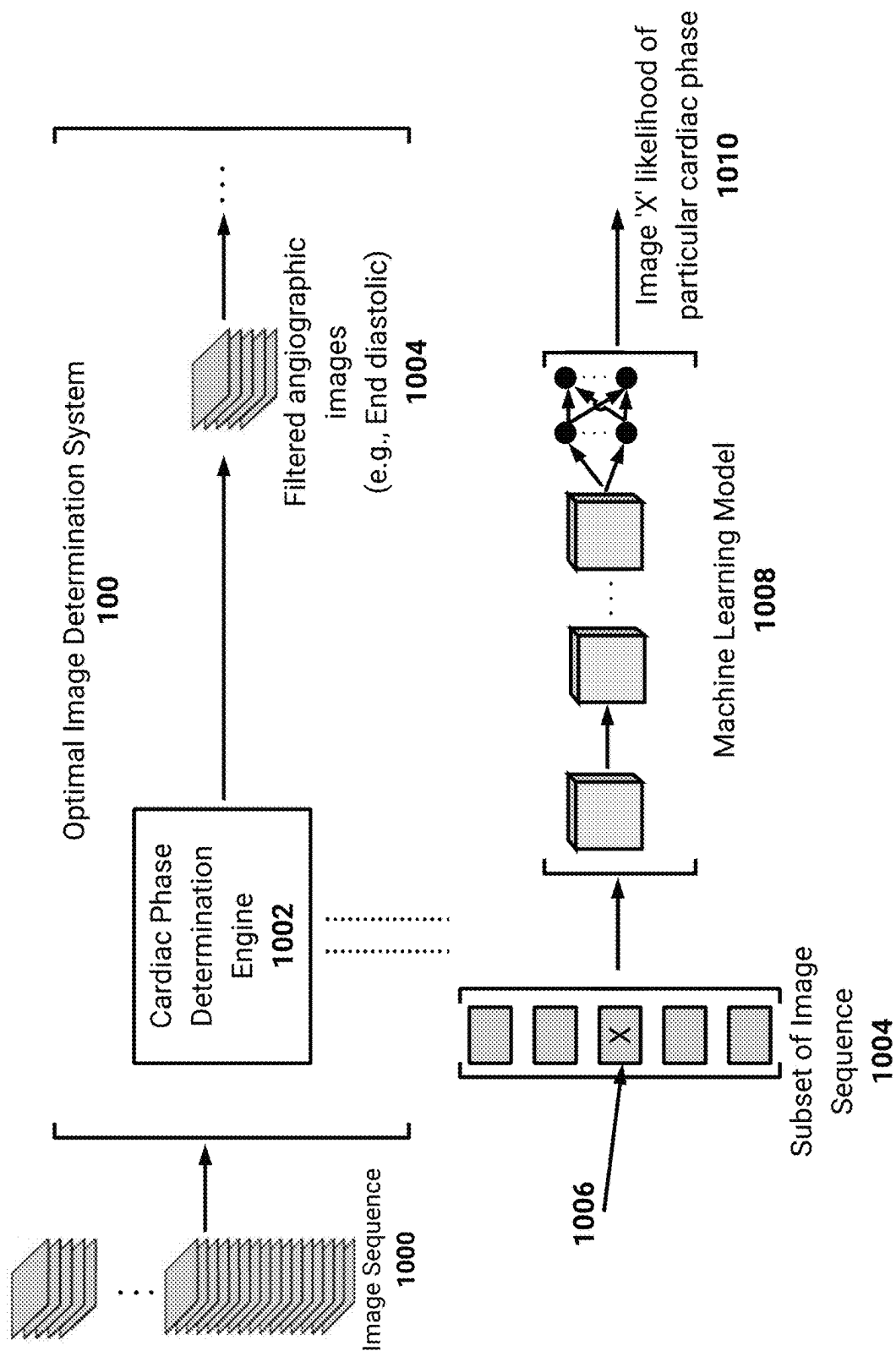


FIG. 10A

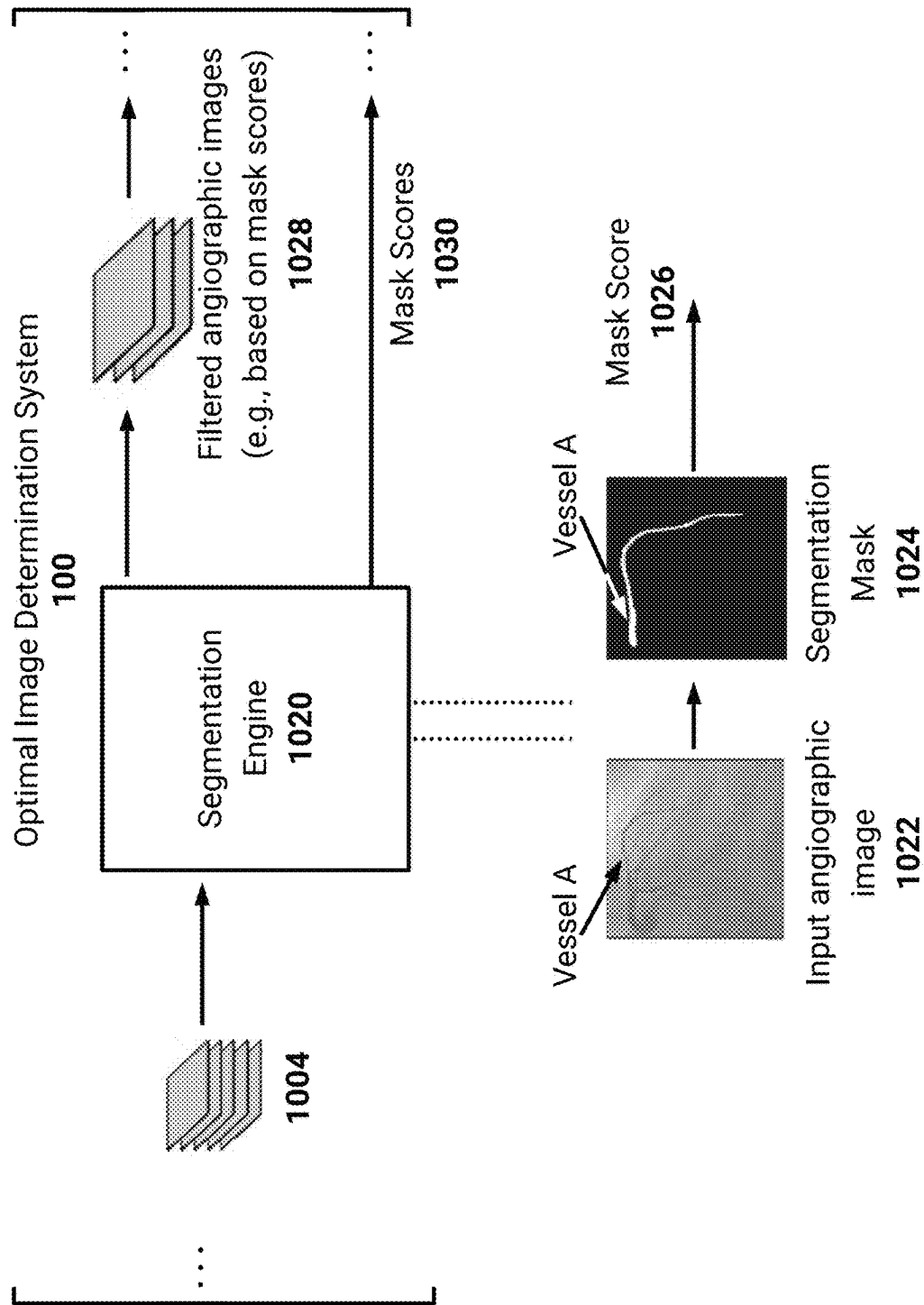


FIG. 10B

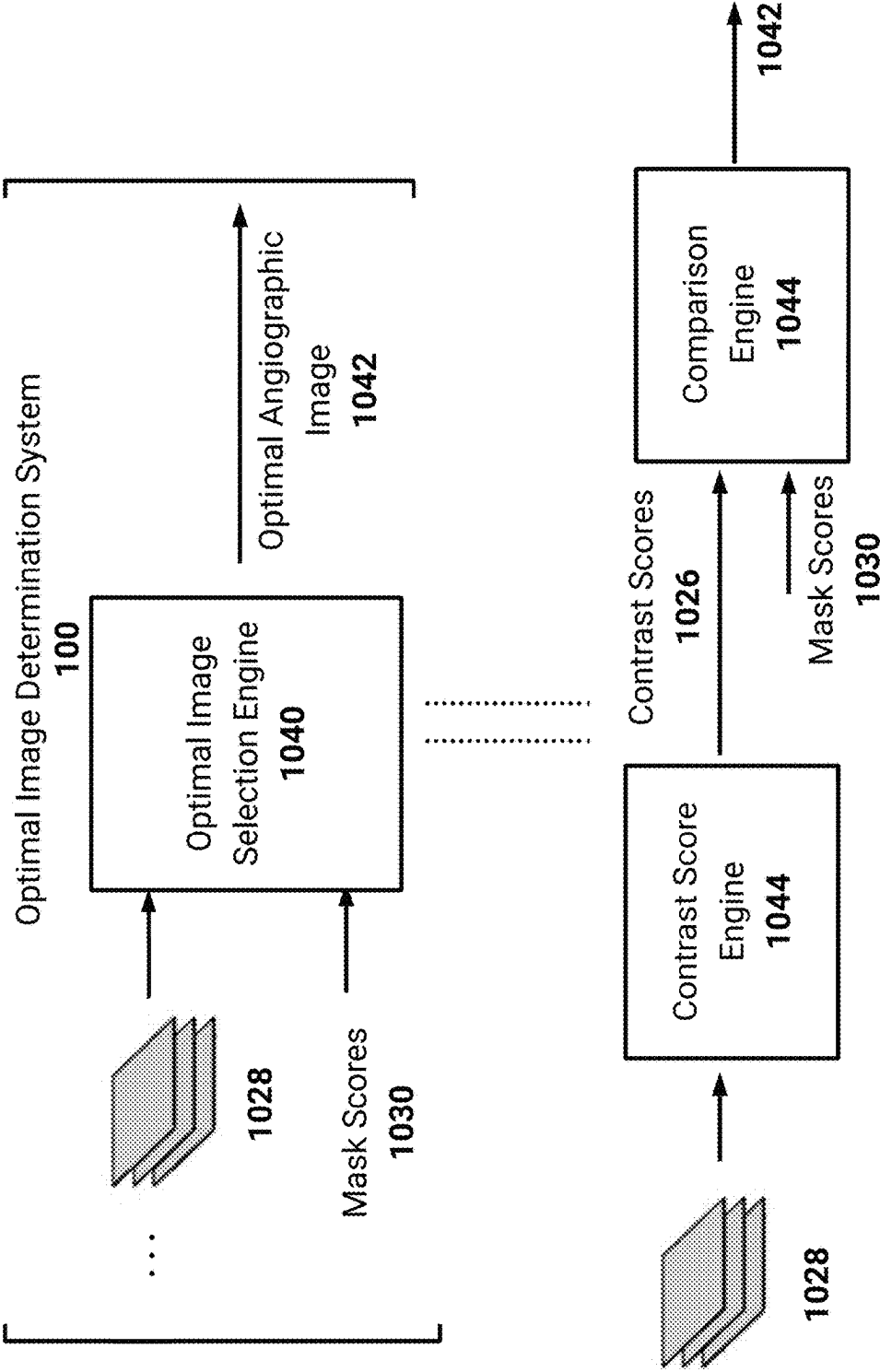


FIG. 10C

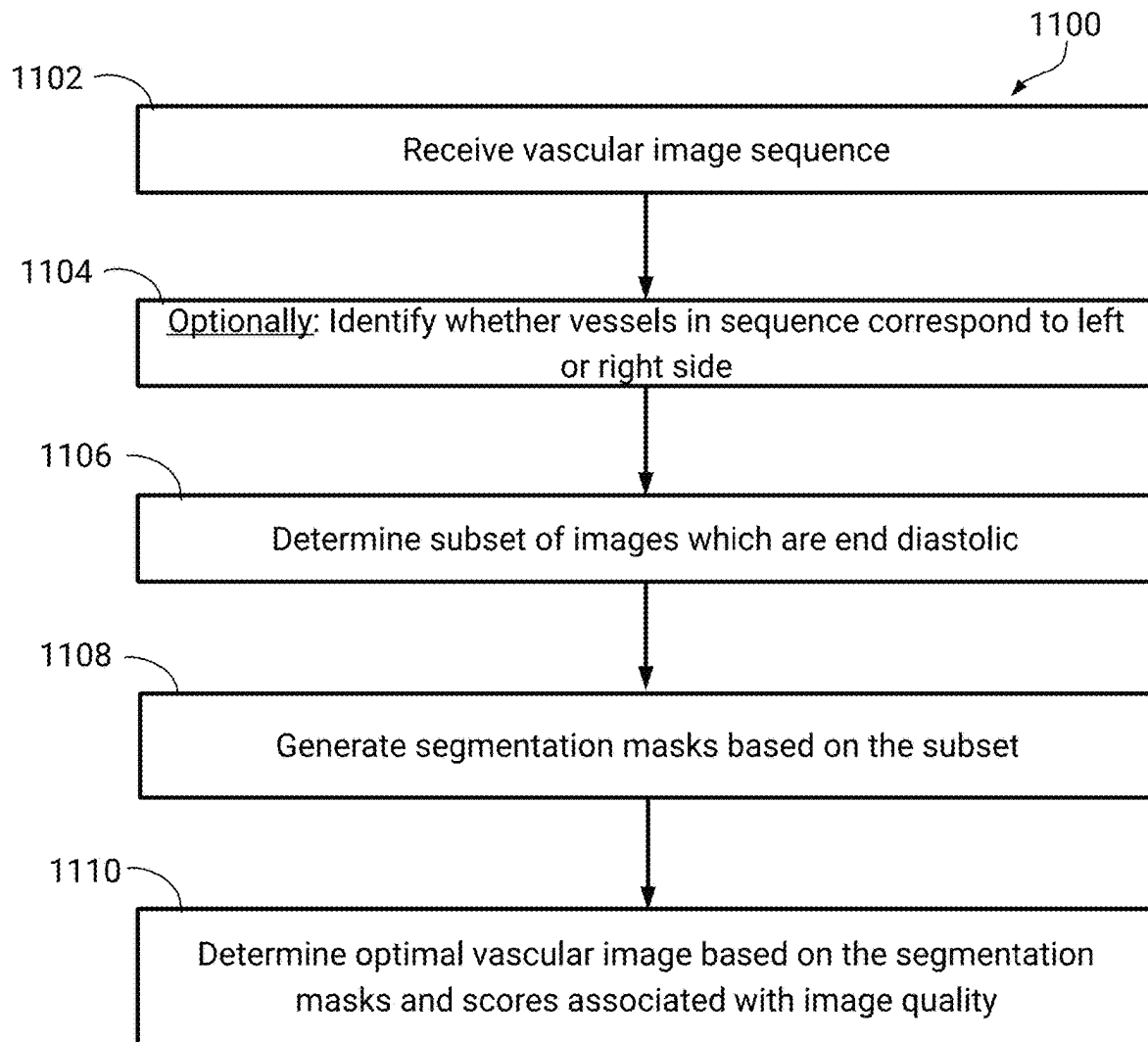


FIG. 11

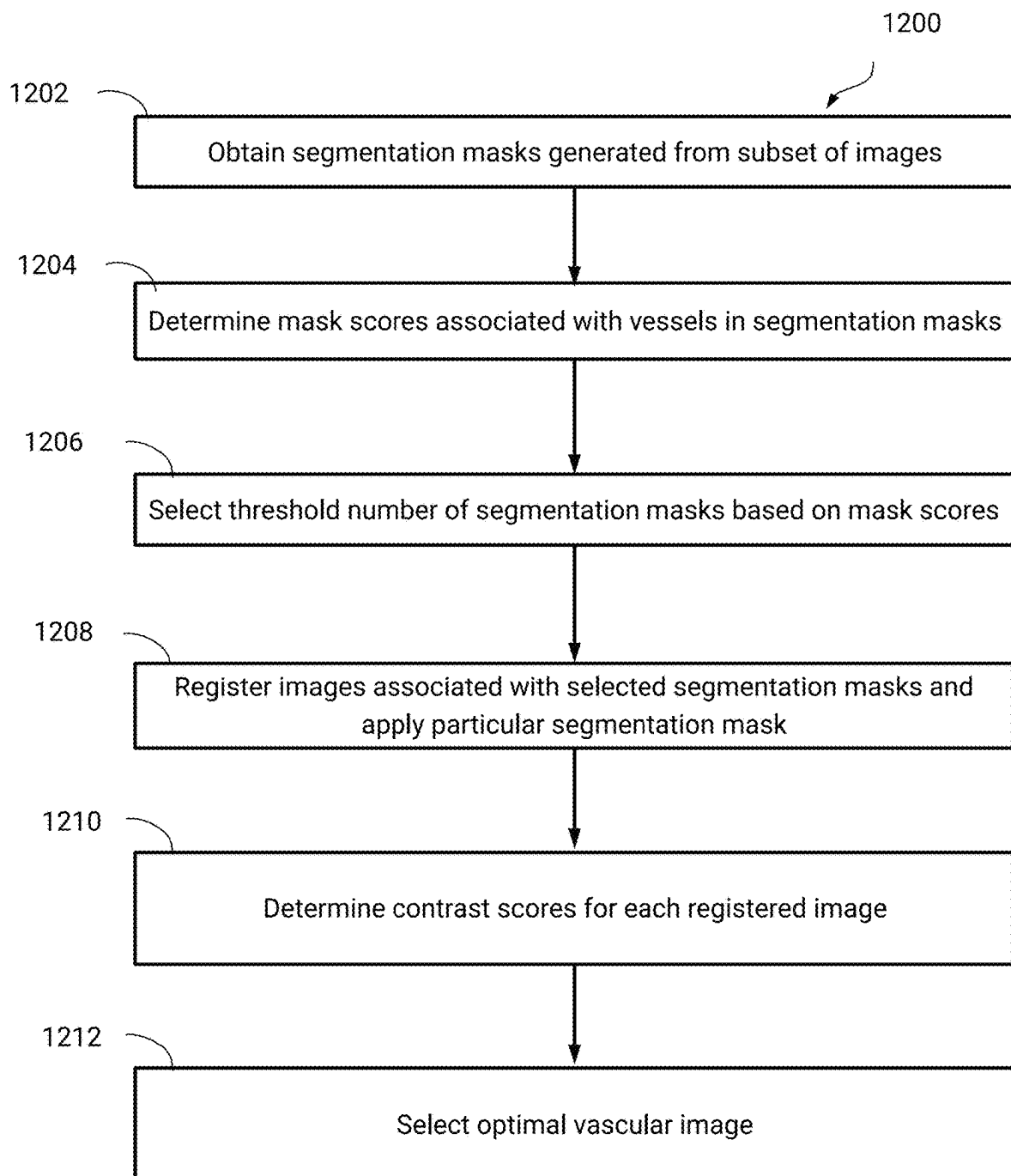


FIG. 12

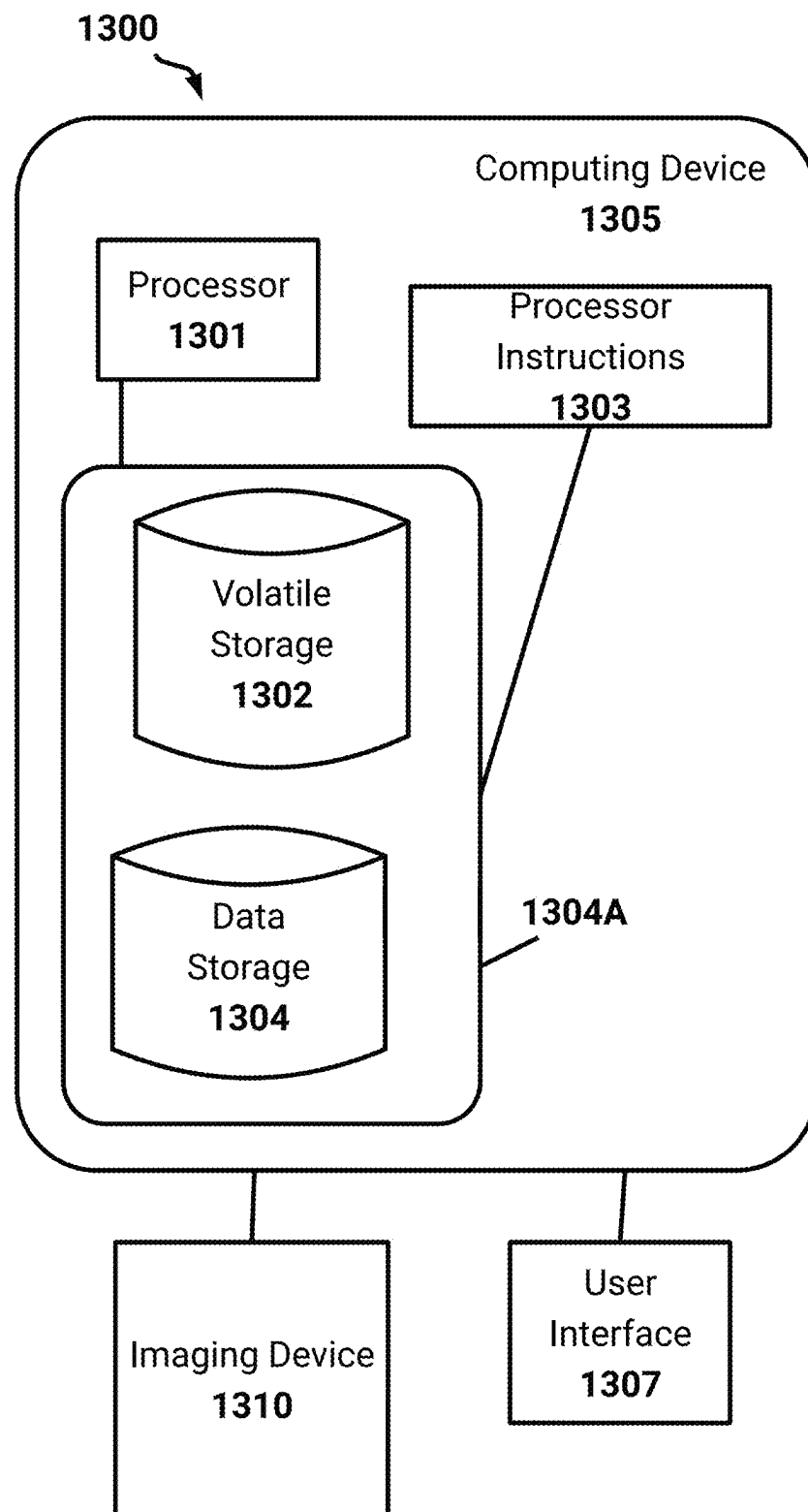


FIG. 13

1

SYSTEM AND METHOD FOR MACHINE-LEARNING BASED SENSOR ANALYSIS AND VASCULAR TREE SEGMENTATION

CROSS-REFERENCE TO RELATED APPLICATIONS

Any and all applications for which a foreign or domestic priority claim is identified in the Application Data Sheet as filed with the present application are hereby incorporated by reference under 37 CFR 1.57.

This application claims priority to U.S. Prov. Patent App. No. 63/308,550 titled "VASCULAR TREE SEGMENTATION" and filed on Feb. 10, 2022, the disclosure of which is hereby incorporated herein by reference in its entirety.

BACKGROUND

Technical Field

The present invention, in some embodiments thereof, relates to the field of vascular imaging and more particularly, but not exclusively, to vascular computer modelling and segmentation.

Description of Related Art

Arterial stenosis is one of the most serious forms of arterial disease. Its severity can be determined by estimations of geometric measurements or flow rate of the vessels, typically through invasive procedures. However, by creating a vascular computer model using images of the vessel, it is possible to determine the severity of an arterial stenosis without the need for invasive procedures. Vascular imaging provides characterizations of blood vessel locations needed to generate a vascular computer model. However, vascular imaging requires vascular segmentation and feature identification as a preliminary stage of image-based measurement of the vascular state.

Currently, many stages of vascular segmentation and feature identification can be performed using an automated analysis. Automatic identification of vascular positions is a potential advantage, since it can reduce the time, effort, skill, and/or attention required of a human operator to identify these positions entirely manually, even if the user must manually confirm or correct a vascular tree afterwards.

Despite the ability to perform automated analysis, relevant image features produced from vascular segmentation and feature identification are often of low contrast. The image features may also be embedded in a complex environment including elements of ambiguous geometry and extraneous features that causes the output to be error prone.

BRIEF DESCRIPTION OF THE DRAWINGS

Throughout the drawings, reference numbers are re-used to indicate correspondence between referenced elements. The drawings are provided to illustrate embodiments of the subject matter described herein and not to limit the scope thereof.

FIG. 1 is a block diagram of an optimal image determination system outputting an optimal angiographic image based on an input image sequence.

FIG. 2 is a schematic diagram of different algorithmic components from among which vascular identifiers may be selected, according to some embodiments of the present disclosure.

2

FIGS. 3A, 3B, 3C, 3D, 3E, 3F, 3G and 3H depict an X-ray angiogram image (depicted in each of FIGS. 3A, 3C, 3E, and 3G) together with different mask-type ML-based vascular identifier outputs (FIGS. 3B, 3D, 3F, 3H) corresponding to different anatomically distinct vascular types, according to some embodiments of the present disclosure.

FIG. 4 shows two superimposed path-type ML-based vascular identifier outputs, according to some embodiments of the present disclosure.

FIGS. 5A-5B schematically represent a method of vascular identification repair using mixed path-type and mask-type ML-based vascular identifiers, according to some embodiments of the present disclosure.

FIGS. 6A, 6B, 6C, 6D, 6E, 6F, 6G and 6H depict an X-ray angiogram image (depicted in each of FIGS. 6A, 6C, 6E, and 6G) together with different mask-type ML-based vascular identifier outputs (FIGS. 6B, 6D, 6F, 6H) corresponding to different anatomically distinct vascular types, according to some embodiments of the present disclosure.

FIG. 6J shows two superimposed path-type ML-based vascular identifier outputs, according to some embodiments of the present disclosure.

FIG. 6K shows a segmented result, produced based on the use of the various correct and partially incorrect information available from the ML-based vascular identifier outputs shown in FIGS. 6B, 6D, 6F, 6H, and 6J, according to some embodiments of the present disclosure.

FIGS. 7A, 7B, 7C and 7D depict an X-ray angiogram image (depicted in each of FIGS. 7A and 7C) together with different mask-type ML-based vascular identifier outputs (FIGS. 7B, 7D) corresponding to different anatomically distinct vascular types, according to some embodiments of the present disclosure.

FIG. 7E shows a path-type ML-based vascular identifier output superimposed on the image of FIGS. 7A-7C, according to some embodiments of the present disclosure.

FIG. 7F shows a segmented result, produced based on the use of the various correct and partially incorrect information available from the ML-based vascular identifier outputs shown in FIGS. 7B, 7D, and 7E, modified by further constraints, according to some embodiments of the present disclosure.

FIGS. 8A, 8B, 8C, 8D and 8E schematically illustrate exchange of vascular orientation information from a path-type ML output to a mask-type ML-based vascular identifier output, according to some embodiments of the present disclosure.

FIGS. 9A, 9B, 9C, 9D, 9E, 9F and 9G schematically illustrate a method of performing vascular subtraction between mask-type vascular identifier outputs, according to some embodiments of the present disclosure.

FIG. 10A illustrates a block diagram of the example optimal image determination system filtering angiographic images according to cardiac phase.

FIG. 10B illustrates a block diagram of the example optimal image determination system performing additional filtering based on mask scores associated with segmentation masks.

FIG. 10C illustrates a block diagram of the example optimal image determination system generating an optimal angiographic image.

FIG. 11 is a flowchart of an example process for determining an optimal angiographic image.

FIG. 12 is a flowchart of an example process for selecting an optimal angiographic image from an image sequence based on contrast scores.

FIG. 13 is an example system which may be used to implement the techniques described herein.

DETAILED DESCRIPTION

Introduction

This application describes, among other things, techniques to select a vascular image, from a sequence of vascular images, which provides enhanced contrast, enhanced visibility of vessels, enhanced image quality, and so on. As will be described, the selected vascular image may be used for further analyses, such as forming a three-dimensional model of at least a portion of a patient's heart. The selected vascular image may also be used as part of an automated process or workflow in which a user can identify vessels in the vascular image, adjust an automated determination of vessels in the vascular image, and so on. The vascular images described herein may represent angiographic images in some embodiments, with each sequence of vascular images depicting the portion of the patient's heart from a particular viewpoint. As may be appreciated, combining vascular images from different viewpoints may allow for a three-dimensional view of the portion to be generated. At present such three-dimensional views are prone to inaccuracies due to the vascular images suffering from movement errors, differences in cardiac phases when the images were obtained, and so on. This disclosure describes techniques to optimize, or otherwise enhance, the selection of a subset of these vascular images to reduce such inaccuracies.

As will be described, a system described herein may implement one or more machine learning models, optionally in conjunction with classical computer vision techniques, to determine an optimal image from among a multitude of inputted vascular images. The system may be, for example, the optimal image determination system 100 described below. For example, a machine learning model may include a neural network (e.g., a deep learning model, a convolutional neural network). In this example, the system may compute a forward pass through the machine learning model to generate output utilized in the determination. In some embodiments, the neural network may output segmentation masks for at least some of the received vascular images. These segmentation masks may segment vessels depicted in the vascular images.

The system may analyze the above-described segmentation masks, for example determining size or length scores associated with depicted vessels. Using these scores, the system may select a top threshold number of images. The system may analyze the threshold number of images to identify an optimal image. For example, the system may compute contrast scores indicating measures of contrast or other image quality for the vessels depicted in the images. The optimal image may represent, in some embodiments, an image with the highest scores or combination of scores. Through this automated selection of an optimal image, resulting downstream workflows such as three-dimensional model generation may allow for enhanced accuracy while lessening the need and time spent for manual adjustments by a human operator post-analysis.

Introduction—Background

Angiographic images are commonly used to provide detailed views of a patient's heart. These images may be obtained, for example, by injecting a radio-opaque contrast agent into the patient's blood vessels and obtaining X-ray images (e.g., via fluoroscopy). While these images provide

detailed views, due to the use of X-rays medical professionals may prefer to limit an extent to which angiographic images are obtained. Thus, it is paramount that techniques are employed for downstream processes which accurately leverage existing angiographic images.

One example downstream process includes generating a three-dimensional model, or vascular tree, of a portion of patient's heart. For example, angiographic images of different views of the portion may be obtained. In this example, the different views may depict different views of vessels. As known by those skilled in the art, these vessels may be correlated to identify unique vessels depicted in the views. For example, automated or semi-automated techniques may be leveraged to allow for such correlation. The views may be combined to generate a three-dimensional view of these vessels. The views may also be combined to allow for an easy-to-understand graphical representation of a vessel tree which indicates vessels which are upstream and/or downstream from each other.

Typically, an image sequence of angiographic images will be obtained while an imaging system (e.g., a c-arm) is pointing at the portion of the patient's heart. For example, 5, 10, 20, and so on, angiographic images may be obtained. As may be appreciated, these angiographic images may vary in their usefulness with respect to the above-described downstream processes. For example, a subset of the angiographic images may have errors due to movement or shaking of the imaging system. As another example, a subset may have errors associated with contrast. As another example, the angiographic images may depict the portion of the heart as the heart is in different cardiac phases. For this example, certain cardiac phases may be associated with less detail, size, and so on, of vessels in the resulting angiographic images.

Additionally, errors or ambiguities may relate to:

- Use of angiographic images which are two-dimensional projections of complex three-dimensional vasculature, creating the spurious appearance in single images of vascular connections which don't actually exist.

- Potentially, blood vessels hide one another due to overlap. Contrast agent used to reveal the vasculature may fill blood vessels of interest incompletely, unevenly, weakly and/or sporadically.

- Indications of other body structures, and sometimes out-right artifacts may appear in the image, creating image "noise" which interferes with identification of targets of interest.

- There are technological and/or safety limitations on image resolution and radiant energy exposure, which can limit, for example, image detail and/or contrast.

- Cardiac vasculature moves with the beating of the heart and/or respiration, and the patient may themselves move; so that there is even a problem of selecting which 3-D shape of the vasculature is to be reconstructed.

Typically, a user of a software tool may view images in an image sequence and select one which appears to depict the vessels most clearly. For example, the user may zoom into the images and identify potential errors which are evident in these images. Certain software tools may allow for limited automated techniques to surface potential errors. For example, classical computer vision techniques may be used to detect motion artifacts.

In contrast, the disclosed technology leverages machine learning models specifically trained to address such errors and ambiguities.

Introduction—Optimal Image Selection

The system includes one or more machine learning models, such as convolutional neural networks, which are used by the system to output a particular angiographic image from an image sequence which will be used in downstream processes. The particular angiographic image is referred to as an optimal angiographic image or image frame herein.

For example, the system receives an image sequence from an angiographic imaging tool or system (e.g., a c-arm). In this example, the imaging tool or system may be rotated such that angiographic images depict, or otherwise include, a portion of a patient's heart from a particular viewpoint. The image sequence may thus include angiographic images taken at different points in time from the particular viewpoint.

The patient's heart will beat and therefore transition between cardiac phases. The angiographic images in the image sequence may therefore depict the portion of the patient's heart in different cardiac phases. For example, a first image may depict the heart while it is in a systole phase. As another example, a second image may depict the heart while it is in a diastolic phase. As known by those skilled in the art, the second image may provide a clearer, more advantageous, view of vessels in the portion of the heart. For example, the second image may depict the portion as being lengthened and in more of a relaxed state as compared to the first image.

As will be described, the system may leverage machine learning techniques to identify images in the image sequence which depict the heart in a particular cardiac phase. In some embodiments, the particular cardiac phase may be an end-diastolic phase. The machine learning techniques may include a convolutional neural network which is trained to label, or otherwise indicate a value indicative of, an image depicting the heart in the particular cardiac phase. While a convolutional neural network is described, as may be appreciated other machine learning models may be used. For example, fully-connected networks, recurrent neural networks, attention-based networks, and so on may be used.

The system may then use machine learning techniques, or optionally classical computer vision techniques (e.g., application of a Frangi filter, and so on), to output segmentation masks for these identified images. For example, the segmentation masks may have pixel values assigned based on whether the pixel forms part of a vessel. In this example, a segmentation mask may include binary color (e.g., black, and white) with a first color indicating a pixel which does not form part of a vessel and a second color indicating a pixel which does form part of a vessel. While binary colors are described, as may be appreciated each pixel may be assigned or value or likelihood indicative of the pixel forming part of a vessel.

The segmentation masks may then be analyzed to identify size or length metrics associated with vessels (herein referred to as 'mask scores'). For example, a mask score may indicate a length associated with a vessel. In this example, the length may indicate a length associated with a centerline from a first end of a vessel to a second end of the vessel. As another example, a mask score may indicate a fill score (e.g., an area) associated with a vessel. In this example, the fill score may indicate a number of pixels which form the vessel, or an estimated area encompassed by the vessel. Use of the mask scores allows for removal of images where a contrast agent fills the patient's vessels incompletely, unevenly, weakly, and/or sporadically. For example, these images may have segmentation masks which include vessels appearing in disconnected segments or with

reduced length or size. A threshold number of the segmentation masks may be maintained, for example 3, 5, 7, 9, 10, 12, and so on may be maintained as having the greatest mask scores.

The system may then analyze angiographic images which were used to generate the threshold number of segmentation mask. For example, the system may determine quality or clarity scores for the angiographic images. Quality or clarity scores are described herein as contrast scores and are used to indicate images with the best contrast. While contrast scores are described herein, additional quality or clarity scores may be used and fall within the scope of the disclosed technology. For example, scores associated with one or more of sharpness, focus, motion artifacts, image artifacts, and so on, may be used. An optimal image may then be selected from the analyzed angiographic images based on the quality or clarity scores.

As described in FIG. 1, the optimal image may be presented to an end-user in a user interface. In some embodiments, the end-user may view the optimal image and use it for down-stream processes. For example, the end-user may mark, or otherwise identify, vessels in the optimal image. The end-user may also select a different image from the above-described image sequence.

In some embodiments, and as will be described, different machine learning models may be used based on whether the image sequence depicts a left side of right side of the patient's heart. For example, the left-side images may depict the left anterior descending artery (LAD) and the circumflex artery (LCX) while the right-side images may depict the right coronary artery (RCA). In some embodiments, a machine learning model (e.g., a convolutional neural network) may be used to indicate whether the image sequence depicts the left-side or right-side. For example, the machine learning model may output a classification.

The disclosed technology therefore addresses technical problems and provides technical solutions to these problems. For example, there may be no need to unnecessarily increase image resolution or radiant energy exposure during X-rays due to the intelligent selection of angiographic images. As another example, use of machine learning models allows for accurate classification and determination of information to reliably select an optimal image from an image sequence. Without such techniques, resulting three-dimensional models of a heart, or information derived from angiographic images, may include errors and inaccuracies which negatively affect patient outcome.

In this disclosure, the term "ML-based vascular identifier" refers to machine learning outputs. The term "vascular identifier" more generally encompasses both ML-based vascular identifiers and computer processing-based methods of identifying vascular regions in images (e.g., formula-based methods, such as classical computer vision techniques). Example classical computer vision techniques may include a kernel filter (e.g., a skeletonization filter or Gaussian filter), an affine transform (e.g., a combination of translation, scaling, rotation, flipping and/or shear), a bit mask, a component analysis technique (e.g., principle component analysis), and a domain transform (e.g., a Fourier transform between frequency and spatial domains). In particular, in some embodiments of the present disclosure, a version of a filter type known in the art as a Frangi filter is used to assist in detecting the generally tubular structures of which vasculature is composed.

In this application, and as an example, FIGS. 1 and 10A-12 may be relevant to techniques for determining an optimal image frame from an image sequence. FIGS. 2-9G

may be relevant to techniques for determining vessels in vascular images based on segmentation masks, addressing errors in determining vessels and/or segmentation masks, and so on. In some embodiments, the optimal image may be analyzed via the techniques described in FIGS. 2-9G to accurately identify vessels associated with vessel trees or arteries (e.g., left or right arteries), address errors, and so on. Thus, the system described herein may determine an optimal image and then analyze the image, for example via segmentation masks or other ML-based vascular identifier outputs, as described in FIGS. 2-9G.

These and other features will now be described in detail. Block Diagram

FIG. 1 illustrates a block diagram of an optimal image determination system 100. The system 102 may represent, for example, a system of one or more computers or processors which implements the techniques described herein. In some embodiments, the system may be in communication with an imaging system or tool which obtains vascular images of a patient. As described herein, the vascular images may be angiographic images. In some embodiments, the vascular images may be computed tomography images or scans.

In the illustrated embodiment, the optimal image determination system 100 is receiving an image sequence 102 which includes angiographic images 104A-104N. The image sequence 102 may depict a portion of a patient's heart from a certain angle or viewpoint. The angiographic images 104A-104N can be obtained, in some embodiments, by user input. For example, the user may input a DICOM file which includes a series of angiographic images or a video from which the angiographic images can be extracted. The images 104A-104N may be captured at a particular frequency (e.g., 5 Hz, 7 Hz, 10 Hz, 30 Hz, and so on) over an amount of time, resulting in potentially large numbers of images.

The images 104A-104N may be taken during a period of vascular contrast agent injection and washout. As already described, within a single image, there may arise ambiguities in vascular structure due to vascular portions which cross and/or approach each other. Since the heart is hollow, and since X-ray images image all through the heart, some of these ambiguities arise from blood vessels which are actually in completely different 3-D planes (e.g., on opposite sides of the heart). As a result, blood vessels which appear to be near each other in a static 2-D plane may nonetheless have different patterns of motion, inconsistent with them actually lying within the same tissue bed. This inconsistency may be viewed as latent information about vascular connectivity. Another form of temporal information arises from the dynamics of vascular filling. Blood vessels which connect to one another should be highly correlated in the dynamics of their filling (darkening) and emptying (lightening) upon injection of vascular contrast agent, and then again as the contrast agent washes out. Unconnected blood vessels, even if they appear to intersect in an image, may be less correlated in their filling dynamics.

In view of these ambiguities, certain angiographic images in the sequence 102 may provide a clearer, and more accurate, depiction of vessels in the patient's heart. Thus, the optimal image determination system 100 may determine an optimal image 110 from the image sequence 102 which represents the best image from a particular angle or viewpoint. As will be described, for example with respect to at least FIGS. 10A-12, the optimal image may be identified using machine learning techniques optionally in combination with classical computer vision techniques. For example, the optimal image may have an optimal, or otherwise

aggregate best, combination of features including, for example, size of depicted vessels, clarity of the image, connectedness of vessels, and so on. With respect to connectedness, the optimal image may depict a vessel as being substantially continuous without separations.

The optimal image 110 may be used by an end-user as medical data for example downstream processes. For example, the system 100 may identify locations, or boundaries, of vessels in the optimal image 110. In this example, the end-user may adjust these locations or boundaries and optionally identify locations or boundaries of other vessels in the image 110. As another example, the end-user may obtain multiple (e.g., 2, 3, 5, and so on) optimal images from different image sequences. For this example, the end-user may cause a three-dimensional model or vascular tree to be generated. Thus, the optimal images may represent images determined to be the most advantageous for use in these down-stream processes from their respective image sequences.

In FIG. 1, a user interface 120 is illustrated as including optimal image 110. The user interface 120 may be generated, in some embodiments, by the system 100. For example, the system 100 may execute software which causes presentation of the user interface 120. The user interface 120 may also be presented by a user device of the end-user. For example, the system 100 may provide information for inclusion in the user interface 120 as rendered by the user device. In this example, the system 100 may be in wired or wireless communication with the user device. As an example, the system 100 may be associated with a web application.

In some embodiments, the user interface 120 may include a button or other selectable object 122 to cause selection of a different optimal image. For example, the end-user may select button 122 to view other angiographic images in the image sequence 102. In this example, the user interface 120 may update to present at least some of these angiographic images. The end-user may thus override the optimal image 110 to select a different optimal image. In some embodiments, such an override may be used to update the machine learning models described herein.

The user interface 120 may be used, for example, to identify an image sequence for analysis. For example, the end-user may provide user input which causes the user interface 120 to respond to selection of an image sequence. Once selected, the selection of the image sequence may trigger the system 100 to determine an optimal image as described herein. The optimal image may then be shown or otherwise included in the user interface 120 as illustrated in FIG. 1. In some embodiments, an animation or movie may play in the user interface 120 with the animation or movie being formed based on the image sequence. The optimal image may be identified, for example highlighted, text presented proximate to it, or the animation or movie may pause on the optimal image for a threshold amount of time while playing. In this way, the end-user may view the optimal image in the context of the image sequence. As described above, the end-user can select a different optimal image. For example, the end-user may interact with button 122. As another example, the end-user may select an image during the animation or movie of the image sequence.

Another example downstream process may include, for example, a certain image location as being part of a blood vessel (a "vascular portion"), a certain image location as being part of a particular (anatomically identified) blood vessel, a certain image location as being more particularly part of a path definition extending along vascular portions (e.g., a general or anatomically identified vascular center

line), a certain image location as being a “root” location of a vascular tree (e.g., an ostium of a coronary artery), and/or of a certain image or image portion as being a suitable target for another image processing method.

From image inputs (e.g., image inputs showing discernible structural features of cardiac vasculature), a vascular identifier may produce a data structure in which there is some correspondence with positions in the image, e.g., a 1:1 correspondent between identifications and pixels (other types of scaled, binned, or otherwise transformed correspondences are not excluded). The data structure may be in any form of representation suitable to describe identification results; for example, scalar, array, matrix, linked list, or another form of representation. More particularly, the data structure may be a mask; for example, a binary image with a pixel per pixel of the input image, values of mask pixels being set according to the identification result of corresponding input image pixels. In some embodiments, the data structure is a list of locations in the input image which have (or do not have) a certain identification (e.g., identified as representing a portion of a certain vascular centerline). Image locations may be expressed, for example, as absolute locations, or as locations relative to other locations. A path through an image, for example, may be expressed as either of a binary image mask or a list of image locations. A vascular identifier may optionally produce a data structure which performs classification of an image as a whole. For example, the data structure may classify the image according to its likelihood of being an image obtained near a certain phase of the heartbeat cycle.

Types of Vascular Identifiers/Vascular Identifier Outputs

FIGS. 2-9G describe example techniques which may be implemented using the optimal image determination system 100 described herein. As will be described, the system 100 may generate output (e.g., ML-based vascular identifiers, vascular identifiers) which may be included in a user interface (e.g., user interface 120). In some embodiments, an ML-based vascular identifier may include a segmentation mask generated from an angiographic image. A ML-based vascular identifier may also represent, in some embodiments, output from a machine learning model such as score, value, likelihood, classification, and so on.

Reference is now made to FIG. 2, which is a schematic diagram of different algorithmic components from among which vascular identifiers may be selected, according to some embodiments of the present disclosure. The diagram is form of Venn diagram, wherein regions of the diagram (“type-regions”) are characterized by which labeled closed-boundary regions they fall within. The type-regions represent groups of algorithmic components with properties indicated by the labels, and further described herein.

Type-regions 201, 202 represent, respectively, the generic types of ML-based vascular identifiers and formula-based vascular identifiers, respectively, which should be understood in either case as being vascular identifiers available for and suitable for use in the identification of vasculature from vascular image. More particularly, in some embodiments, the vascular identifier is suitable for use in the identification of contrast-agent filled cardiac blood vessels in X-ray angiogram images of a living heart.

Within either of the type-regions 201, 202 may be distinguished more particularly a type-region 203 of mask-type vascular identifiers and a type of region 204 path-type vascular identifiers (representations of type-regions 203, 204 are split among type-regions 201, 202 to reduce visual clutter). Mask-type vascular identifiers, herein, are understood to be vascular identifiers that provide output which

expresses a likelihood (optionally a threshold likelihood) of a particular image pixel being in or not in a suitably defined vascular target. Characteristics of mask-like vascular identifier outputs include:

Being non-directional, e.g., the vascular identifier output as such does not indicate vascular orientation.

Being “blobby”—that is, having width of arbitrary size in any direction from any particular point within the mask.

The output from a path-type vascular identifier in contrast, is directional; for example, locations identified are in an order which the vascular identifier output defines. The path, moreover, is skeletal (not blobby); e.g., having no representation of width as such.

It should be noted that the outputs of mask-type and path-type vascular identifiers can be inter-converted by various processing methods to have the directionality/blockiness of the opposite type. For example, a blob can be skeletonized, and a path can have different widths assigned to locations along its longitudinal extent. What is counted herein for purposes of type-region assignment is the form of the initial classification. Parenthetically, it may be also noted that a vascular identifier could, in principle, combine even within its initial classification, both the directionality of a path-type output and the arbitrary width of a mask-type output (that is, these two properties are not logically incompatible). Nor is it excluded that there are vascular identifiers sharing none of the distinguishing properties of path-type and mask-type vascular identifiers. However, unless otherwise noted, vascular identifiers used in the examples given can be reasonably understood as belonging to one of the two types just given.

Corresponding to the initial classification type, there may be understood to be an underlying difference in how mask-type and path-type vascular identifiers use the information available to them which traces to differences in their underlying models. In particular, path-type vascular identifiers operate based on the model assumption that there is a path—an ordered set of locations which extend between a starting position and an ending position. From the further knowledge or assumption that two non-adjacent locations are on the path, a path-type vascular identifier relies on there being a third location between them. The model of a mask-type vascular identifier may work from model assumptions that assess pixel properties and patterns without reliance on such global properties.

It is not forbidden for embodiments of the present disclosure that a vascular identifier may use (for example) both path-like information and pattern-like information to produce its output, and this may be true even if the output itself is strictly path-type or mask-type). Indeed, and particular in the case of for an ML-based vascular identifier, it may be difficult to restrict, and perhaps infeasible to determine what type of information is being used. However, even in that case, it may be understood that the use of path-type training data vs. mask-type training data will tend to influence the training process that produces the ML-based vascular identifier, so that path-like or pattern-like information is emphasized to a greater or lesser degree.

Accordingly, in some embodiments of the present disclosure, there is provided for use a mask-type vascular identifier. The mask-type vascular identifier may be in turn an ML-based vascular identifier. In some embodiments, the vascular identifier is more particularly characterized by having a classification-type output layer (e.g., as a member of type-region 206), as also described hereinabove. The mask-type ML-based vascular identifier may be one trained

using mask data, with the mask data identifying which portions of a vascular image should be considered as vascular portions.

In some embodiments, the mask-type vascular identifier is a formula-based vascular identifier, for example, a Frangi filter-based vascular identifier **207** (AF Frangi et al., “Multiscale Vessel Enhancement Filtering”, Medical Image Computing and Computer-Assisted Intervention—MICCAI’98 Lecture Notes in Computer Science 1496/1998: 130). Variations of this method have also been described in more recent literature. More general examples of formula-based mask-type vascular identifiers include edge detectors and threshold detectors. The Frangi filter-based vascular identifier (and its variations) may be characterized as “tube detectors”, insofar as they are designed to highlight image features which correspond to the image appearance of tubes (which are characteristic of vasculature), such as their possession of a direction of greater longitudinal extent, their possession of a more-or-less constant or slowly changing diameter, their cross-sectional brightness profile, and/or other properties.

Additionally, or alternatively, in some embodiments of the present disclosure, there is provided for use a path-type vascular identifier. The path-type vascular identifier may in turn be an ML-based vascular identifier. In some embodiments, the vascular identifier is more particularly characterized by having a regression-type output layer (e.g., as a member of type-group **205**), as also described hereinabove. The path-type ML-based vascular identifier may be one trained using path data, with the path data identifying locations lying along vascular portions. In some embodiments, the locations identified are vascular centerlines. The centerlines are optionally and advantageously identified as representing the geometrical center of blood vessels; however, there is no general restriction requiring this. In some embodiments, additionally or alternatively, the path locations identified are vascular edges.

In some embodiments, the path-type vascular identifier is a formula-based vascular identifier **208**. Such a path-type vascular identifier may, for example, proceed away from a seed location, travelling in one or two directions along the minimum gradient of the image’s local brightness values. When the seed location is within a blood vessel (e.g., a dark blood vessel against a brighter background), this may tend to constrain the direction of travel to be about parallel to the direction of the blood vessel itself, insofar as the vessel is relatively narrow (making a steep gradient) compared to its length (along which the gradient is shallower). The path may also trend toward the vascular center since lower overall intensity levels there may also lead to lower gradients. Refinements to this general idea may include different methods of selecting seed locations, resolving stopping conditions, and/or bridging vascular crossings and/or gaps in vascular brightness.

Apart from its usefulness in description of some embodiments of the present disclosure, the distinction between path-type and mask-type vascular identifiers is of relevance to the problem of vascular identification because it allows pointing out—more generally—that even though two vascular identifiers may both be designed to solve the same problem of “identifying blood vessels” in an image, their underlying model differences drive them to somewhat different solutions.

In the case of two ML-based vascular identifiers, this can be true even when the vascular identifiers were trained using the same basic underlying images. This is, in turn, practically important, because any given vascular identifier is likely to make a certain number of mistakes. It will identify

a blood vessel where there is none or fail to do so when one should have been identified. Furthermore, the pairing of path-type and mask-type vascular identifiers provides an example of two different types of vascular identifier which tend to make different mistakes. An understanding of the differences there can be converted in turn to a solution which allows complementary use of a plurality of vascular identifiers to achieve results more accurate than any individual vascular identifier (or type of vascular identifier) alone.

The principle of complementarity can be carried more generally to other type-distinctions, including some indicated in FIG. 2. For example, in some embodiments, one or more ML-based vascular identifiers are trained to identify a selective anatomical target, consisting, e.g., not of blood vessels generally (e.g., as may be true of generic/“branched-tube” selective ML-based vascular identifiers **210**), but more particularly of a particular, anatomically defined vascular target such as the LAD, LCX, RCA, and/or sub-tree vessels thereof (these are examples of targets which may be designated for anatomical target selective ML-based vascular identifiers **212**). It should be emphasized that there is no particular technological limitation which prevents training ML-based vascular identifiers of the generic type **210**, or on a somewhat more selective type such as cardiac vasculature generally. However, the inventors have found that training ML-based vascular identifiers on an anatomically restricted range of blood vessels has potential advantages for accuracy of identification and/or the amount of training data needed to reach an acceptable level of accuracy. There may be a further advantage when reconstructing 3-D positions of blood vessels using images taken from different angles. If it is clear which blood vessel is, e.g., the LAD or LCX in each image, then the problem of matching blood vessel coordinates is potentially simplified and/or made less error prone.

Another potential advantage of such an approach is that whatever the vessel-type specialized ML-based vascular identifier identifies as vascular is by this fact also identified as belonging to a particular anatomically defined vascular type. Identification may be relevant, e.g., for analysis of vascular pathologies, wherein the severity of the pathology is judged in part based on which anatomically identified portion of the vasculature is pathological.

The ability of machine learning techniques to create anatomically selective vascular identifiers by suitable selection of training data is, moreover, a potential advantage over the use of formula-based vascular identifiers. For formula-based vascular identifiers, the parameters available for adjustment are not necessarily suited to making anatomical selections of the type needed. For example, Frangi-based algorithms typically have a free parameter which can be adjusted to tune which vascular diameter(s) are detected. However, cardiac blood vessels of interest such as the LAD and LCX not only tend to share similar vascular widths, but also themselves vary in width along their length—so a single width, or range of widths, is not particularly distinguishing. While it may be possible to develop a distinguishing vascular identifier, given sufficient investigation, formula-based vascular identifiers expose no pre-existing “knob” (parameter) which is equivalent in flexibility to the adjustment of training data which is available in the generation of ML-based vascular identifiers.

Anatomically Selective ML-Based Vascular Identifiers Mask-Type ML-Based Vascular Identifiers

Reference is now made to FIGS. 3A-3H, which depict an X-ray angiogram image (depicted in each of FIGS. 3A, 3C, 3E, and 3G) together with different mask-type ML-based vascular identifier outputs (FIGS. 3B, 3D, 3F, 3H) corre-

sponding to different anatomically distinct vascular types, according to some embodiments of the present disclosure. FIG. 3B shows an LAD mask, FIG. 3D shows an LCX mask, FIG. 3F shows a mask comprising the LAD sub-tree (the LAD and its diagonals or branches), and FIG. 3H shows a mask comprising the LCX sub-tree (the LCX and its marginals or branches).

Each of FIGS. 3B, 3D, 3F, 3H was generated from the same image input using a different respective ML-based vascular identifier trained using a training data set specific for the vascular type identified. In some embodiments, the training data set of a given ML-based vascular identifier comprises a large set of images (e.g., more than 1000 images, more than 10000 images, or another number of images), for each of which a mask is defined identifying the targeted, anatomically identified vascular type.

It may be readily understood that from this set of images, each of the LCX and the LAD are distinguishable from the rest of their respective sub-tree vessels by observing which vascular regions in the whole sub-tree vascular identifier output only, and which are in the corresponding single-vessel ML-based vascular identifier's output as well. However, the images potentially require additional algorithmic processing to realize this distinction. Thus, four different vascular types may be identified in a single image, based on the application of four different ML-based vascular identifiers to the image.

It should be noted that the identifications shown in this set of examples are relatively error-free, although it may be noted, e.g., that FIG. 3F shows a small number of disconnected blobs, at least some of which appear to be more appropriately identified as part of the LCX sub-tree. Following examples will describe various types of detection errors in the ML-based vascular identifier outputs, and how they may be addressed through combinations of vascular identifier outputs.

Path-Type ML-Based Vascular Identifiers

Reference is now made to FIG. 4, which shows two superimposed path-type ML-based vascular identifier outputs **401**, **402**, according to some embodiments of the present disclosure. Path **401** extends along the LCX, and path **402** extends along the LAD.

In this case, the ML-based vascular identifiers used were of the regression type, and training data used were not blob-like masks, but rather paths. In part, regression type training proceeds by "teaching" the ML-based vascular identifier to adjust output path positions to reduce deviation in position from paths in the training set, which is a type of regression problem. The trained vascular identifiers are then expected to produce useful vascular identifications when provided with image data not used as part of their training data set. The path has an ordering of locations along the output path, including two path ends. The model may output the path as a sequence of X and Y coordinates.

In some embodiments, more particularly, to apply the path-type ML-based vascular identifier, each of 50 coordinates along a seed starting path is converted to a profile image, and the profile images stacked so that a 2-D image is created. Each profile image comprises pixels perpendicular to the vessel direction and passing through the selected coordinate. In the profile image, the true vascular path extends generally along the seed starting path, but it "wiggles". The ML-based vascular identifier operates by moving seed path coordinates laterally to positions which are considered more likely to actually lie upon the vascular path (optionally also somewhat constrained by the lateral positioning of nearby points, to maintain at least some

amount of contiguity). Optionally, this is performed on an interpolated image, e.g., so that 200 or more (for example, 210) interpolated points are generated. Since the positions of points along the lateral lines are known in the original 2-D image, the laterally moved positions can be mapped back into 2-D image coordinates to give the 2-D shape of the vascular path. Optionally, remapping uses fewer points than were available in the interpolated intermediate image; for example, remapping may return to 50 selected anchor points, and draw the vascular path between anchor points. Anchor points may be connected by straight lines, by spline fits, or by another method.

It may be noted that identifications of paths **401**, **402** substantially overlap with the mask identifications made in FIGS. 3D, 3B, respectively. In some embodiments, pixels in the sub-tree masks of FIGS. 3H, 3F are divided into their main vessel vs. branch vessel types based on comparison with paths **401**, **402** additionally, or alternatively to, comparison with the mask-type outputs of FIGS. 3D, 3B. This is a form of cross-vascular identifier mixing of outputs which combines outputs of path-type ML-based vascular identifiers and of mask-type ML-based vascular identifiers.

Cross-Type Repair Using ML-Based Vascular Identifiers

Reference is now made to FIGS. 5A-5B, which schematically represent a method of vascular identification repair using mixed path-type and mask-type ML-based vascular identifiers, according to some embodiments of the present disclosure.

In FIG. 5A are shown two overlying LCX identifications produced as outputs of ML-based vascular identifiers. Path **501** represents an output of a path-type ML-based vascular identifier, while mask **502** is the output of a mask-type vascular identifier. Each output includes at least one error. Gap **503** is an error in mask **502**, such as may be caused, for example, by a lesion which interferes with contrast agent intensity and/or vascular morphology (the gap has been artificially introduced for purposes of explanation).

Path **501** crosses over gap **503**. Path-type ML-based vascular identifiers can be relatively resistant to local irregularities, since (for example) if there is "normal" vasculature on either side of the gap, the processes of regression will tend to match the path to those normal regions. The region in-between will be bridged as a matter of course, in order to maintain the overall integrity of the path.

However, tail region **504** of path **501** diverges from mask **502**. In some embodiments, deviations of mask **502** and path **501** near the tail **504** are treated as more likely (and optionally necessarily) due to errors in the path **501**. The reason for this may be, for example: that path **501** may be constrained by an over-learned feature such as a limitation on how tortuous the path is allowed to be; a relatively increased sensitivity to small collateral branches; and/or in general a vulnerability to falling into local minima which tends to propagate along the path once an error occurs (previous path dependence).

FIG. 5B illustrates a corrected vascular identification combining mask **502** and path **501**. The tail region **504** can be deleted, for example, because in some portion (most distally) it leaves but never rejoins a portion of mask **502**, or because (slightly more proximally) it leaves and rejoins mask **502**, but it rejoins the same self-connected "blob", and so is not bridging any gap.

In contrast, bridge **505** is retained, for example based on the criterion that two different (not previously interconnected) blobs are bridged. Additionally, or alternatively, other criteria are applied, for example, a maximum bridging

distance and/or similarity of directionality between a skeletonized version of mask **502** and regions of path **501** extending alongside.

ML-Based Vascular Identifier Repair by Combination Example

Reference is now made to FIGS. **6A-6H**, which depict an X-ray angiogram image (depicted in each of FIGS. **6A**, **6C**, **6E**, and **6G**) together with different mask-type ML-based vascular identifier outputs (FIGS. **6B**, **6D**, **6F**, **6H**) corresponding to different anatomically distinct vascular types, according to some embodiments of the present disclosure. FIG. **6B** shows an LAD mask, FIG. **6F** shows an LCX mask, FIG. **6D** shows a mask comprising the LAD sub-tree (the LAD and its diagonals or branches), and FIG. **6H** shows a mask comprising the LCX sub-tree (the LCX and its marginals or branches). In this example, FIGS. **6D** and **6F** each show significant gaps in the detected mask, compared to what can be seen in the X-ray angiogram image.

Further reference is made to FIG. **6J**, which shows two superimposed path-type ML-based vascular identifier outputs **601**, **602**, according to some embodiments of the present disclosure. Path **601** extends along the LCX, and path **602** extends along the LAD. However, path **602** has mostly been misidentified; it has “jumped” to a wrong vessel.

Additional reference is made to FIG. **6K**, which shows a segmented result **603**, produced based on the use of the various correct and partially incorrect information available from the ML-based vascular identifier outputs shown in FIGS. **6B**, **6D**, **6F**, **6H**, and **6J**, according to some embodiments of the present disclosure.

In some embodiments, the rules of combination which result in the segmentation of FIG. **6K** are as already described for the simpler cases before. Path-type segmentation portions which leave but never return to a corresponding mask-type segmentation of the image may be disregarded in the final result. However, where gaps have been spanned by a path-type output result to join two otherwise disconnected mask-type “blobs”, the result can be unified into a single segment. Although this is not illustrated, segments can also be distinguished from each other by knowing which anatomically defined vascular type(s) are being identified by each mask-type or path-type ML-based vascular identifier.

ML-Based Vascular Identifier Repair by Combination and Heuristics Example

Reference is now made to FIGS. **7A-7D**, which depict an X-ray angiogram image (depicted in each of FIGS. **7A** and **7C**) together with different mask-type ML-based vascular identifier outputs (FIGS. **7B**, **7D**) corresponding to different anatomically distinct vascular types, according to some embodiments of the present disclosure. FIG. **7B** shows an RCA mask, and FIG. **7D** shows a mask comprising the RCA sub-tree (the RCA and its diagonals or branches). Further reference is made to FIGS. **7E**, which shows a path-type ML-based vascular identifier output **701** superimposed on the image of FIGS. **7A-7C**, according to some embodiments of the present disclosure. Additional reference is made to FIG. **7F**, which shows a segmented result **703**, produced based on the use of the various correct and partially incorrect information available from the ML-based vascular identifier

outputs shown in FIGS. **7B**, **7D**, and **7E**, modified by further constraints, according to some embodiments of the present disclosure.

In FIG. **7B**, the mask-type ML-based vascular identifier of the RCA yields an erroneous loop **702**, which is due to a branch of the RCA crossing back in front of or behind the RCA itself. The error also appears in the ML-based vascular identifiers which produced the outputs of FIGS. **7D** and **7E**, so that they do not have the information needed to correct each other. However, the basic information that there is an error can be derived from the pattern in FIG. **7B**, since the ML-based vascular identifier there is supposed to identify just a single vessel, and a single vessel should not have any such loop **702**.

Nonetheless, the error can be resolved, based on mask morphology. For example, the mask of FIG. **7B** can be subjected to skeletonization, allowing the locations of bifurcation (top of loop **702**) and crossing (bottom of loop **702**) to be identified. Moving away from those intersection locations, the width of the mask can be identified perpendicular to directions along which the skeletonized mask extends. Of the two branch choices, the branch that better matches the pre-branch (or post-branch) width may be considered as the more likely extension of the RCA. Additionally, or alternatively, intensities in the original image may be used to help assess similarity of vascular morphology. Optionally, locations of bifurcation vs. crossing are distinguished by the extra darkening due to cross-over of vessels that generally is not present at a branch point.

Additionally, or alternatively, the directionality of the two loop branches may be determined leading toward the locations so bifurcation/crossing. Again, this directionality may be determined from a skeletonized version of the mask. The loop branch for which directionality is most nearly parallel to the pre- and/or post-loop branch of the mask may be considered as the more likely extension of the RCA.

In this example, an analysis such as just described allows assigning the short side of loop **702** as part of the RCA itself. This in turn allows assignment of remaining vascular portion identifications based on the ML-based vascular identifier output, for example, to yield the vascular segmentation **703** shown in FIG. **7F**.

It should be understood that the analysis just described is heuristic in character. Heuristics, while often valuable, tend toward a “brittleness”, in that they focus on a particular metric which is assumed to mean something (e.g., mean something about vascular geometry), even though in realistic circumstances, it might not always guarantee what is being assumed for it.

Even with a plurality of heuristics, there can arise situations wherein the heuristics are contradictory, or even agree but yield an incorrect result. Accordingly, there is a potential advantage to reducing the number of ambiguities which need to be resolved heuristically by shifting as much of the vascular segmentation and identification burden as possible to a detector such as an ML-based vascular identifier which is relatively specialized, on one hand (e.g., specialized to detect a particular target type), but also relatively robust in its ability to weight different image features in order to reach a correct vascular identification. The robustness may arise, for example, from the having been generated from realistic examples far more numerous than an algorithm designer could take into individual consideration.

For example, it is noted that the mask of FIG. **7D** could also be used as a basis for rationalizing bifurcations/cross-overs into a simply branched (loop-free) structure. However, the situation becomes more complex because there are

additional logical possibilities that must be excluded. For example, in the example shown, a single RCA branch loops twice across the RCA itself. But near the second crossing **704**, the RCA somewhat constricts, so that from width alone, it may be ambiguous whether the RCA really continues straight across, or else begins a tortuous region by curving to the right. The directionality heuristic might yield a different result, but this results in a potential deadlock unless one of the two heuristics is given priority.

In this case, the directionality heuristic would be correct, but it is not generally infallible. It may be noted, for example, that the bend which a bend to the right at crossing **704** would require is similar in angle to the angle of the next downstream tortuosity **705** in the branched vessel. Should both RCA branch and RCA begin a tortuous region near the region of their closest approach, the directionality heuristic could yield an incorrect result.

Thus, an algorithm designer using a formula-based heuristic approach needs to decide how to prioritize or weight heuristics. Rigorous determination of the correct method of comparison may be impractical, for example due to uncertainty about how relatively important given heuristic weaknesses are. A machine-learned vascular identifier has the advantage of being produced by a process of automatic adaptation to actual results.

In short, the more loops which must be resolved using heuristics, the greater is the opportunity for error. In the case of the example of FIGS. **7A-7F**, the use of an ML-based vascular identifier specialized for single vessel detection has reduced the number of crossing points requiring heuristic resolution compared to the whole sub-tree ML-based vascular identifier's result.

Transfer of Vascular Orientation from Path-Type to Mask-Type Vascular Identifier Outputs

Reference is now made to FIGS. **8A-8E**, which schematically illustrate exchange of vascular orientation information from a path-type ML output to a mask-type ML-based vascular identifier output, according to some embodiments of the present disclosure.

Mask-type output as such detects vascular regions in or out of a certain type of blood vessel (e.g., the LAD or the RCA), but is not inherently oriented to determine which end is the ostium (upstream of proximal side of an artery), and which is the distal end of the artery.

FIG. **8A** shows a mask-type ML-based vascular identifier output detecting the extent of an LAD. FIG. **8B** is a corresponding path-type ML-based vascular identifier. The path-type vascular identifier output is ended, since it is derived from a path model also having ends. The ends themselves may have been labeled as relatively upstream (ostial) or downstream (distal) based on information implicit in how the paths were learned, and/or based on comparison to the result of yet another vascular identifier, for example, a thresholded Frangi filter heat map, wherein the Frangi filter can be tuned to find larger (and therefore more ostial) blood vessels differentially (e.g., preferentially) compared to smaller blood vessels.

In FIG. **8B**, the mask has been skeletonized to skeletonized mask **801**, which can be done by an erosion filter. In FIGS. **8C** and **8D**, a path-type ML-based vascular identifier result **802** is aligned to skeletonized mask **801**. FIG. **8C** shows a magnified portion from near the ostium end of path-type ML-based vascular identifier result **802**. The arrow **803** indicates the distance between the extreme ostial end of path-type ML-based vascular identifier result **802** (for which end information is available), and the closest end of

skeletonized mask **801**. This end becomes the skeletonized mask's ostial end. The opposite end is the distal end.

The path of skeletonized mask **801** is optionally used as a representation of the vascular centerline. Alternatively, the skeletonized mask is used to create a geodesic distance transform of the original mask-type output, and the centerline defined as the shortest path along the geodesic transform between the positions of the ostial and distal ends of the skeletonized mask **801**. The centerline is then transformed back into Cartesian coordinates, for example as shown in FIG. **8E**.

Vascular "Subtraction" in Vascular Masks

Reference is now made to FIGS. **9A-9G**, which schematically illustrate a method of performing vascular subtraction between mask-type vascular identifier outputs, according to some embodiments of the present disclosure. In the example shown, the vascular identifier outputs are outputs of two different ML-based vascular identifiers, which distinguish the LAD (FIG. **9A**) and the LAD and its diagonals (FIG. **9B**), respectively.

FIG. **9C** shows the result of a simple mask subtraction, with bright pixels being those found in the mask of FIG. **9B** alone, dark pixels being those found in the mask of FIG. **9A** alone, and gray pixels being either found in both masks, or in neither. The subtraction result is unsatisfactory, since it leaves a fringe of mixed black and white pixels where the two ML-based vascular identifiers reached slightly different results as to where the edges of the LAD should be placed.

FIG. **9D** shows the image from which the masks of FIGS. **9A-9B** were derived. As a stage of addressing the "fringe" problem, contrast enhancement has been applied to the region of the mask of FIG. **9B**. The contours of this enhanced region are shown in FIG. **9E**, the contours having been calculated only within the vicinity of pixels which are portions of the LAD (alone) mask. This may be accomplished, for example, by dilating the mask of FIG. **9A** until it slightly over-fills contours of the whole enhanced region, and then only retaining contours in contact with the dilated mask. FIG. **9F** shows the resulting LAD mask, and FIG. **9G** shows the difference mask retaining a branch of the LAD sub-tree.

Example Machine Learning Techniques—Block Diagram/Flowcharts

FIGS. **10A-13** describe examples of determining an optimal image from an image sequence of angiographic images. Similar to FIGS. **2-9G**, the description of which is relevant to these figures, the optimal image determination system **100** may perform the techniques described below.

FIG. **10A** illustrates a block diagram of the example optimal image determination system **100** filtering angiographic images according to cardiac phase. The optimal image determination system **100** operates by filtering an image sequence **1000** to those which include angiographic images associated with a particular cardiac phase. In some embodiments, the system **100** filters the sequence **1000** to include images which are end diastolic.

As illustrated, the optimal image determination system **100** includes a cardiac phase determination engine **1002** which analyses the image sequence **1000**. In some embodiments, the cardiac phase determination engine **1002** may be a machine learning model **1008** which receives a subset **1004** of the image sequence **1000** as input. For example, the subset **1004** may include 1 image, 3 images, 5 images, and so on. With respect to 5 images, a center image **1006** may be combined (e.g., concatenated) with two subsequent, and two previous, images in the image sequence **1000**.

The system **100** may compute a forward pass through the machine learning model **1008** and obtain a likelihood, or value, associated with the center image **1006** depicting the heart during a particular cardiac phase. In some embodiments, the machine learning model **1008** may represent a neural network which is trained to assign a value indicative of a likelihood (e.g., a final layer may use a sigmoid activation function). With respect to the example of 5 input images, as may be appreciated the neural network may effectively learn to distinguish movement indicia of the heart, such as expansion, which are associated with the particular cardiac phase. The neural network may also be trained to assign a classification associated with a cardiac phase. The neural network may include, for example, a convolutional neural network, a fully-connected neural network, an attention-based network, a recurrent neural network, and so on.

With respect to a recurrent neural network, the model **1008** may be a long short-term memory (LSTM) network. Use of LSTM units may allow the model **1008** to exploit temporal information associated with the image sequence **1000**. Additionally, LSTM units may help distinguish vessels and their localization using information about how they change (e.g., move and/or move relative to one another) over time, or simply information about how well another ML-based vascular identifier identifies them in a sequence of images.

As described above, end diastolic images may be preferable as they capture when the blood vessels are at their largest. For example, the cardiac phase corresponds to when the ventricles of the heart are most expanded. This image is relatively identifiable since it occurs during the moments of transition between expansion and contraction of the heart. Therefore, this can assist with matching to other images obtained during later or earlier heartbeat cycles, since there is less likely to be differences in heart shape due to heart contraction.

In the illustrated example, the cardiac phase determination engine **1002** has output filtered images **1004** which are associated with the particular cardiac phase (e.g., end-diastolic images). For implementations which use a likelihood or probability of the particular cardiac phase, the engine **1002** may filter (e.g., remove or discard) images which received a likelihood or probability less than a threshold (e.g., 60%, 75%, 90%).

FIG. **10B** illustrates a block diagram of the example optimal image determination system **100** performing additional filtering based on mask scores associated with segmentation masks. As described in FIG. **10A**, the system **100** may analyze angiographic images included in an image sequence and identify a subset **1004** which depict the heart during a particular cardiac phase (e.g., an end-diastolic phase). As will be described, the system **100** may further refine or filter the subset **1004** using segmentation masks which indicate image portions depicting vessels.

The optimal image determination system **100** includes a segmentation engine **1020** which outputs a segmentation mask based on an input of an angiographic image. For example, in FIG. **10B** the segmentation engine **1020** has received an input angiographic image **1022**. As illustrated, the input angiographic image **1022** depicts one or more vessels (e.g., 'Vessel A'). The resulting segmentation mask **1024** depicts the one or more vessels, such as Vessel A, as being segmented from the remainder of the image **1022**. In some embodiments, the segmentation mask **1024** may include pixels assigned binary values by the segmentation engine **1020**. A first binary pixel value, such as white, may

indicate that the pixel forms part of a vessel. A second binary pixel value, such as black, may indicate that the pixel does not form part of a vessel.

While FIG. **10B** illustrates the segmentation mask **1024**, as may be appreciated in some embodiments the segmentation engine **1020** may output information identifying the vessel's location or position in the input image **1022**. For example, the engine **1020** may output a data structure (e.g., a vector or other information) which identifies pixels forming a vessel. As another example, the engine **1020** may output information indicating a boundary or contour of a vessel.

The segmentation engine **1020** may represent a machine learning model which is trained to output segmentation masks. For example, a convolutional neural network may be trained to output segmentation **1024**. In this example, the convolutional neural network may be trained based on ground truth segmentation masks and associated angiographic images. In some embodiments, the segmentation engine **1020** may represent performance of classical computer vision techniques. As described herein, the neural network may be specific to a side or artery of the heart. For example, a first neural network may output segmentation masks for images associated with a right-side of the heart. As another example, one or more additional neural networks may output segmentation masks for images associated with a particular artery of a left-side of the heart (e.g., a left anterior descending, left marginal, left circumflex artery).

These segmentation masks may be of the mask-type or path-type, as described in FIG. **2**. In overview, mask-type outputs comprise "blobs" of connected pixels which are categorized as belonging to a certain vascular type, but not necessarily structured except insofar as their connectivity can be used for further analysis procedures such as skeletonization. Path-type outputs arrange regions along a path in a definite order, typically with the ends themselves also being identified, e.g., as closer to the ostium, or more distal from it (e.g., relatively upstream/downstream, respectively in the case of arteries). Additionally, and as described in FIGS. **2-9G**, the segmentation masks may be analyzed to address errors or update information in the masks.

In some embodiments, at least one formula-based method (e.g., classical computer vision technique) is combined with at least one machine-learning based method. For example, a Frangi filter can be utilized in conjunction with the segmentation network to identify smaller unidentified vessels missed by the segmentation network. More particularly, the edgeClearFrangi (ECF) Frangi filter variant may be used. A Frangi filter is a formula-based method used to generate a "heat map" giving a likelihood of given pixels being vascular, and optionally the heat map is converted, for example by application of a threshold, into mask of image pixels judged to be vascular regions. Frames where the Frangi filter is more responsive (e.g., in terms of overall response intensity and/or area of the mask meeting a certain threshold criterion), are correspondingly considered to have greater and/or denser vascular filling with contrast agent. Additionally, the Frangi filter can be used to connect gaps missed by the segmentation network to reduce connectivity problems. Therefore, in addition to reducing connectivity problems that may otherwise remove the image from optimal frame consideration, the Frangi filter will provide an indication to the user that a vessel exists and what its contours are so a user can draw those vessels in post.

Further description related to segmentation masks, and example graphical representations of segmentation masks, are included herein with respect to FIGS. **2-9G**. For

example, the segmentation engine 1020 may output ML-based vascular identifiers such as different mask type outputs.

Based on the segmentation mask 1024, the segmentation engine 1020 generates a mask score 1026 associated with one or more vessels in the mask 1024. For example, the mask score may indicate a measure or metric associated with a size of Vessel A. In this example, the segmentation engine 1020 may determine a number of pixels which form Vessel A (e.g., a number of the white pixels). The segmentation engine 1020 may also determine an area (e.g., an image area) associated with Vessel A. The segmentation engine 1020 may also determine a length of Vessel A. As an example, the length may indicate a length associated with a line which is positioned through the center of Vessel A (e.g., a centerline).

A segmentation mask may incompletely depict a vessel, for example the segmentation mask may have discontinuities or white portions separated by black portions. In some embodiments, the segmentation engine 1020 may correct discontinuities. For example, the engine 1020 may assign a black portion (e.g., a portion indicated as not forming a vessel) as being a white portion if the black portion is below a threshold size or length and adjacent to white portions on one, or both, sides. To correct discontinuities, as an example, the engine 1020 may apply a Frangi filter to the segmentation mask. Correcting discontinuities is additionally described elsewhere, with respect to FIGS. 3A-9G. In some embodiments, the segmentation engine 1020 may discard certain angiographic images in the subset 1004 from further analysis based on inclusion of such discontinuities. Thus, the engine 1020 may prefer angiographic images which result in segmentation masks with reduced errors.

The segmentation engine 1020 may therefore determine masks 1030 scores for the subset 1004. As described above, a mask score may indicate a size or length associated with a vessel. In some embodiments, an image may have a mask score for each vessel depicted in an associated segmentation mask. In some embodiments, an image may have a single mask score which is based on the vessels depicted in the associated segmentation mask.

Using the mask scores 1030, the segmentation engine 1020 may filter the subset 1004. For example, the segmentation engine 1020 may discard angiographic images which are associated with mask scores less than a threshold percent of a maximum (e.g., higher) mask score. Thus, the segmentation engine 1020 may output filtered angiographic images 1028 along with the mask scores 1030.

FIG. 10C illustrates a block diagram of the example optimal image determination system 100 generating an optimal angiographic image 1042. As described in FIG. 10B, the system 100 may determine images 1028 whose associated segmentation masks include lengthy, or larger, vessels. These images 1028 may thus more provide a clearer view of the vessels.

The optimal image determination system 100 includes an optimal image selection engine 1040 which determines, or otherwise outputs, the optimal angiographic image 1042. In some embodiments, the optimal angiographic image 1042 represents one of the images 1028 which has the best image quality. For example, the optimal angiographic image 1042 may have the best contrast.

As illustrated, images 1028 are provided to a contrast score engine 1044. The contrast score engine 1044 may register the images 1028, for example aligning the images. As known by those skilled in the art, aligning the images may allow for them to be properly compared. For example,

slight movements of the imaging tool (e.g., c-arm) or of the patient may result in slight differences between the viewpoints associated with the images 1028. Thus, the same vessel may be positioned differently in the images 1028.

Subsequent to aligning the images, the contrast score engine 1044 may determine contrast scores 1026 for the images 1028. For example, the angiographic images may be in grayscale. In this example, the engine 1044 may determine a contrast score based on a vessel depicted in one of the images 1028. The contrast score may indicate, for example, an average grayscale value. These contrast scores may be generated based on the same vessel as depicted or included in the images 1028.

As an example, once the images are aligned 1028 a same segmentation mask may be used (e.g., applied) to the images. The segmentation mask may thus identify the vessel in the images 1028 and the contrast scores 1026 may be generated using respective image information for the vessel. In some embodiments, the segmentation mask may represent a segmentation mask which is a combination, or aligning of, the segmentation masks determined for the images 1028 in FIG. 10B. In some embodiments, the segmentation masks may be aligned and then combined using a logical 'Or' such that the masks may extend beyond vessels depicted in an image. As may be appreciated, the image may thus have a shorter view of the vessels and, as described below, when computing the contrast score the image may have a lower contrast score due to use of additional non-vessel areas which are darker.

A comparison engine 1044 may then identify the optimal angiographic image 1042 based on the contrast scores 1026 and mask scores 1030. For example, the engine 1044 may select image 1042 as being one of the images 1028 with the highest contrast score 1026. This may indicate that the image 1042 has an acceptable size or length of vessel (e.g., as described in FIG. 10B), and has the best image contrast. As another example, the engine 1044 may use a combination of the contrast scores 1026 and mask scores 1030. For example, the scores 1026, 1030, may be weighted and the highest combination may indicate the optimal angiographic image 1042. Optionally, the mask scores 1030 may be used only upon two or more of the images 1028 having contrast scores 1026 within a threshold.

While FIGS. 10A-10C describe use of machine learning models, as may be appreciated a single machine learning model or multiple machine learning models may be used. For example, a single machine learning model may be end-to-end trained to identify an optimal angiographic image based on a received image sequence. As another example, multiple machine learning models may be used to perform different steps. For example, a first model may be used to identify images which are end-diastolic, and a second model may be used to output segmentation masks. Left-Side/Right-Side Arteries

As known by those skilled in the art, there are two primary coronary arteries—the right coronary artery and the left main coronary artery. The right-side has a main artery, known as the right coronary artery, while the left-side has more than one artery. For example, the left-side bifurcates into the left anterior descending (LAD) artery and the left circumflex artery (LCX). The left circumflex artery has a branch referred to as the left marginal artery (LMA).

In some embodiments, the system 100 may analyze a received image sequence 1000 and identify whether the image sequence 1000 is depicting left-side, or right-side, vessels. For example, the system 1000 may provide each image of the image sequence 1000 to a machine learning

model (e.g., a convolutional neural network, optionally with one or more fully-connected layers). The model may output, for each image, respectively probabilities of the depicted vessels being left-side or right-side. The model may also output a classification indicating whether the vessels are left-side or right-side. The image sequence **1000** as whole is determined to depict the right or left side of the heart according to what the majority of the included angiographic images are determined to be. For example, a voting technique may be used to select a side based on whether the majority of the included images are determined to be left-side or right-side.

Thereafter, the system **100** may use the assigning of left-side or right-side to enhance accuracy of its determinations. For example, in some embodiments the system **1000** may use separate machine learning models to determine images which are end-diastolic. In this example, two machine learning models may be trained using training data specific to the left-side or right-side. Similarly, the system **1000** may use separate segmentation networks or models for the left-side or right-side.

With respect to separate segmentation masks, as described above the left-side may have two or more arteries (e.g., the LAD, and LCX or LMA). For the left-side, the system **1000** may therefore generate two or more segmentation masks. In some embodiments, different segmentation networks may be used for the arteries. As described in FIG. 10C, the system **1000** may determine mask scores based on the segmentation masks. For the left-side, the system **1000** may thus determine two or more mask scores for each image. These mask scores may optionally be combined, or aggregated, into a single mask score for the image. The mask scores may optionally be maintained separately and used to filter images as described above. For example, images which have a mask score less than a threshold percent of a maximum mask score may be discarded.

Example Flowcharts

FIG. 11 illustrates is flowchart of an example process **1100** for determining an optimal angiographic image. For convenience, the process **1100** will be described as being performed by a system of one or more computers or processors (e.g., the optimal image determination system **100**).

At block **1102**, the system receives a vascular image sequence. As described, the system receives vascular images, such as angiographic images, of a portion of a patient's heart. The images may be taken by an imaging system or tool (e.g., a c-arm) at a particular rotation and/or translation about the patient's heart. Thus, the images may be associated with a particular viewpoint of the portion.

At block **1104**, the system optionally determines whether vessels in the image sequence correspond to the left-side or right-side of the patient's heart. In some embodiments, a machine learning model (e.g., a convolutional neural network) may be used to effectuate this determination. For example, and as described above, the machine learning model may output values indicative of respective likelihoods that the vessels are included in the left-side or right-side.

At block **1106**, the system determines a subset of the vascular images which are end diastolic. As part of identifying an optimal image, and as described in FIG. 10A, the system determines vascular images which are associated with a lengthening and/or relaxing of the vessels of the heart. This cardiac phase, such as end diastolic phase, may allow for enhanced downstream processing of the optimal image. For example, an end diastolic phase image may provide added detail and/or clarity of vessels such that an end-user may more rapidly identify, mark, and so on, vessels in the

image. As another example, end diastolic phase images may allow for superior (e.g., less error-prone) three-dimensional modeling.

At block **1108**, the system generates segmentation masks based on the subset. As described in FIG. 10B, the system generates segmentation masks to identify vascular images which depict larger and/or lengthier vessels. For example, while taking certain vascular images the dye may not properly fill into the patient's vessels such that certain vascular images may result in less apparent vessels.

The system generates mask scores based on the segmentation masks. For example, the mask scores may indicate a length or size associated with vessels included in the segmentation masks. The system may then filter, such as remove or discard, images which have less than a threshold percentage of a maximum mask score.

As described above, the system may generate a single segmentation mask for a right-side vascular image and two or more segmentation masks for a left-side image. For example, and with respect to the left-side image, the system may generate a first segmentation mask depicting vessels associated with a left anterior descending artery. The system may similarly generate a second segmentation mask depicting vessels associated with a left marginal artery. These segmentation masks may be analyzed separately or combined into a single mask score as described herein.

At block **1110**, the system determines the optimal vascular image based on the segmentation masks and scores associated with image quality. The image quality scores, as described in FIG. 10C, may be referred to as contrast scores and indicate measures of contrast quality in the vascular images. An example process to determine a contrast score is described in FIG. 12. As described above, the system may thus select the optimal image as having the best image quality. The system may also select the optimal image as having the best combination of image quality and mask score.

The system may output the optimal vascular image for presentation via an interactive user interface as described in FIG. 1. The end-user may review the determined image and optionally select a different vascular image from the sequence. In some embodiments, such overrides may be used to update the machine learning models described herein.

FIG. 12 is a flowchart of an example process **1200** for selecting an optimal angiographic image from an image sequence based on contrast scores. For convenience, the process **1200** will be described as being performed by a system of one or more computers or processors (e.g., the optimal image determination system **100**).

At block **1202**, the system receives obtains segmentation masks generated from vascular images. At block **1204**, the system determines mask scores associated with the vessels depicted in the segmentation masks. At block **1206**, the system selects a subset of the vascular images based on the mask scores.

At block **1208**, the system registers the subset of vascular images. For example, the system aligns the images (e.g., rotates the images, removes portions of the images, and so on) to allow for the subset to have same features or elements (e.g., vessels) in same portions of the images. The system may generate a particular segmentation mask, such as a combination of the segmentation masks (e.g., a sum of the masks), to be universally applied to the subset. In some embodiments, the particular segmentation mask may be an aligning of the segmentation masks. In some embodiments,

the particular segmentation mask may represent a segmentation mask generated from an aligned image.

At block **1210**, the system determines contrast scores for the subset of vascular images. The system applies the particular segmentation mask to each image in the subset to identify the vessels depicted therein. The system then determines the contrast score for an image based on the average grayscale value of the pixels which form the vessels depicted in the image. A lower average grayscale value may indicate, in some embodiments, a higher contrast score.

At block **1212**, the system selects an optimal vascular image as described at least in FIGS. **10C** and **11**.
Example System

Reference is now made to FIG. **13**, which schematically illustrates a system **1300** configured for use in vascular tree segmentation from cardiac images, according to some embodiments of the present disclosure. In some embodiments, the system **1300** may be the system **100** described herein.

Computing device **1305** is a main subsystem of system **1300**. Imaging device **1310** may be provided with system **1300** or may be a separately provided imaging device with which system **1300** is interconnected to allow access to cardiac vasculature images generated by imaging device **1310**. In some embodiments, imaging device **1310** is an X-ray angiography machine.

Computing device **1305**, in some embodiments, comprises processor **1301**. Processor **1301** comprises, collectively, the processing capabilities of the computing device **1305**, and does not imply limitation to either a single processing unit, a single enclosure, or a single processing device type. For example, processor **1301** may mix CPU and GPU processing units; processor **1301** is optionally distributed among processing units linked by network connections. Memory **1304A**, comprises one or both of volatile storage **1302** and data storage device **1304** (again, these blocks comprise, collectively, available memory capabilities of the computing device). Processor instructions **1303** (stored in memory **1304A**) instruct the processor to perform computational aspects of the system's function, for example, computational aspects of one or more of the methods described herein. For example, processor instructions may comprise programming instructions for any one or more of the methods of FIGS. **11** and **12**, and/or instructions for performing any one or more of the methods or techniques described in relation to FIGS. **2-9G**. Memory **1304A**, in some embodiments, encodes a machine learning product which may be a ML-based vascular identifier. In some embodiments, additionally or alternatively, memory **1304A** encodes instructions for carrying out a formula-based algorithm.

Optional user interface **1307** is configured, in some embodiments, to support receiving user-specified instructions to the system, and to provide displays and indications of device function, for example, images of cardiac vasculature and/or segmentations thereof.

Other Embodiments

All of the processes described herein may be embodied in, and fully automated, via software code modules executed by a computing system that includes one or more computers or processors. The code modules may be stored in any type of non-transitory computer-readable medium or other computer storage device. Some or all the methods may be embodied in specialized computer hardware.

Many other variations than those described herein will be apparent from this disclosure. For example, depending on the embodiment, certain acts, events, or functions of any of the algorithms described herein can be performed in a different sequence or can be added, merged, or left out altogether (for example, not all described acts or events are necessary for the practice of the algorithms). Moreover, in certain embodiments, acts or events can be performed concurrently, for example, through multi-threaded processing, interrupt processing, or multiple processors or processor cores or on other parallel architectures, rather than sequentially. In addition, different tasks or processes can be performed by different machines and/or computing systems that can function together.

The various illustrative logical blocks and modules described in connection with the embodiments disclosed herein can be implemented or performed by a machine, such as a processing unit or processor, a digital signal processor (DSP), an application specific integrated circuit (ASIC), a field programmable gate array (FPGA) or other programmable logic device, discrete gate or transistor logic, discrete hardware components, or any combination thereof designed to perform the functions described herein. A processor can be a microprocessor, but in the alternative, the processor can be a controller, microcontroller, or state machine, combinations of the same, or the like. A processor can include electrical circuitry configured to process computer-executable instructions. In another embodiment, a processor includes an FPGA or other programmable device that performs logic operations without processing computer-executable instructions. A processor can also be implemented as a combination of computing devices, for example, a combination of a DSP and a microprocessor, a plurality of microprocessors, one or more microprocessors in conjunction with a DSP core, or any other such configuration. Although described herein primarily with respect to digital technology, a processor may also include primarily analog components. For example, some or all of the signal processing algorithms described herein may be implemented in analog circuitry or mixed analog and digital circuitry. A computing environment can include any type of computer system, including, but not limited to, a computer system based on a microprocessor, a mainframe computer, a digital signal processor, a portable computing device, a device controller, or a computational engine within an appliance, to name a few.

Conditional language such as, among others, "can," "could," "might" or "may," unless specifically stated otherwise, are understood within the context as used in general to convey that certain embodiments include, while other embodiments do not include, certain features, elements and/or steps. Thus, such conditional language is not generally intended to imply that features, elements and/or steps are in any way required for one or more embodiments or that one or more embodiments necessarily include logic for deciding, with or without user input or prompting, whether these features, elements and/or steps are included or are to be performed in any particular embodiment.

Disjunctive language such as the phrase "at least one of X, Y, or Z," unless specifically stated otherwise, is understood with the context as used in general to present that an item, term, etc., may be either X, Y, or Z, or any combination thereof (for example, X, Y, and/or Z). Thus, such disjunctive language is not generally intended to, and should not, imply that certain embodiments require at least one of X, at least one of Y, or at least one of Z to each be present.

Any process descriptions, elements or blocks in the flow diagrams described herein and/or depicted in the attached figures should be understood as potentially representing modules, segments, or portions of code which include one or more executable instructions for implementing specific logical functions or elements in the process. Alternate implementations are included within the scope of the embodiments described herein in which elements or functions may be deleted, executed out of order from that shown, or discussed, including substantially concurrently or in reverse order, depending on the functionality involved as would be understood by those skilled in the art.

Unless otherwise explicitly stated, articles such as “a” or “an” should generally be interpreted to include one or more described items. Accordingly, phrases such as “a device configured to” are intended to include one or more recited devices. Such one or more recited devices can also be collectively configured to carry out the stated recitations. For example, “a processor configured to carry out recitations A, B and C” can include a first processor configured to carry out recitation A working in conjunction with a second processor configured to carry out recitations B and C.

It should be emphasized that many variations and modifications may be made to the above-described embodiments, the elements of which are to be understood as being among other acceptable examples. All such modifications and variations are intended to be included herein within the scope of this disclosure.

What is claimed is:

1. A method implemented by a system of one or more computers, the method comprising:

accessing an image sequence comprising a plurality of vascular images, the vascular images depicting a portion of a heart from a particular viewpoint and the vascular images being associated with different times within a time range;

determining a subset of the vascular images which are associated with a particular cardiac phase, wherein determining comprises computing a forward pass through a machine learning model trained to classify vascular images based on cardiac phase;

generating segmentation masks associated with the subset, wherein the segmentation masks segment vessels included in the respective vascular images which form the subset, wherein mask scores are determined for the segmentation masks which are indicative of a size or length associated with a vessel included in a segmentation mask, and wherein the subset is filtered to remove one or more vascular images based on the mask scores; and

determining a particular vascular image included in the filtered subset, wherein the determination is based analyzing one or more image quality measures determined for each vascular image included in the filtered subset,

wherein the particular vascular image is configured for inclusion in an interactive user interface.

2. The method of claim 1, wherein the vascular images are angiographic images.

3. The method of claim 1, wherein determining a subset of cardiac phase images comprises:

determining whether the image sequence is associated with a left-side or a right-side of the heart,

wherein the machine learning model is selected from a plurality of machine learning models based on the determination.

4. The method of claim 1, wherein the machine learning model is a convolutional neural network, and wherein determining the subset comprises:

obtaining, from the image sequence, a threshold number of the vascular images, wherein the images which form the threshold number are contiguous in the image sequence; and

providing the threshold number of the vascular images as input to the machine learning model, wherein the machine learning outputs a classification associated with a particular image in the threshold number.

5. The method of claim 1, wherein the particular cardiac phase is end-diastolic.

6. The method of claim 1, wherein the segmentation masks are generated based on a different machine learning model, wherein the different machine learning model is trained to segment vessels depicted in vascular images.

7. The method of claim 1, wherein the image sequence is determined to be associated with a left-side or a right-side of the heart, and wherein for the right-side, a single segmentation mask is generated for each vascular image included in the subset.

8. The method of claim 1, wherein the image sequence is determined to be associated with a left-side or a right-side of the heart, and wherein for the left-side, two or more segmentation masks are generated for each vascular image included in the subset.

9. The method of claim 1, wherein a mask score is indicative of a length associated with a vessel or an area associated with the vessel.

10. The method of claim 1, wherein determining a particular vascular image comprises:

registering the vascular images included in the filtered subset, wherein registering comprises aligning features depicted in the vascular images;

determining image quality measures comprising contrast scores for the vascular images included in the filtered subset, wherein a contrast score indicates an average grayscale value associated with vessels in the vascular images; and

determining the particular vascular image based on the contrast scores.

11. The method of claim 10, wherein a unified segmentation mask is generated for the vascular images included in the filtered subset, and wherein the contrast scores compare contrast of same vessels included in the vascular images.

12. The method of claim 1, wherein the interactive user interface is configured to enable selection of a different vascular image than the particular vascular image, and wherein the system is configured to update the machine learning model based on the selection.

13. A system comprising one or more computers and non-transitory computer storage media storing instructions that when executed by the one or more computers, cause the one or more computers to:

access an image sequence comprising a plurality of vascular images, the vascular images depicting a portion of a heart from a particular viewpoint and the vascular images being associated with different times within a time range;

determine a subset of the vascular images which are associated with a particular cardiac phase, wherein determining comprises computing a forward pass through a machine learning model trained to classify vascular images based on cardiac phase;

generate segmentation masks associated with the subset, wherein the segmentation masks segment vessels

29

included in the respective vascular images which form the subset, wherein mask scores are determined for the segmentation masks which are indicative of a size or length associated with a vessel included in a segmentation mask, and wherein the subset is filtered to remove one or more vascular images based on the mask scores; and

determine a particular vascular image included in the filtered subset, wherein the determination is based on analyzing one or more image quality measures determined for each vascular image included in the filtered subset,

wherein the particular vascular image is configured for inclusion in an interactive user interface.

14. The system of claim 13, wherein to determine a subset of cardiac phase images, the instructions cause the one or more computers to:

determine whether the image sequence is associated with a left-side or a right-side of the heart,

wherein the machine learning model is selected from a plurality of machine learning models based on the determination.

15. The system of claim 13, wherein the image sequence is determined to be associated with a left-side or a right-side of the heart,

wherein for the right-side, a single segmentation mask is generated for each vascular image included in the subset, or

wherein for the left-side, two or more segmentation masks are generated for each vascular image included in the subset.

16. The system of claim 13, wherein to determine a particular vascular image, the instructions cause the one or more computers to:

register the vascular images included in the filtered subset, wherein registering comprises aligning features depicted in the vascular images;

determine image quality measures comprising contrast scores for the vascular images included in the filtered subset, wherein a contrast score indicates an average grayscale value associated with vessels in the vascular images; and

determine the particular vascular image based on the contrast scores.

17. Non-transitory computer storage media storing instructions that when executed by a system of one or more computers, cause the one or more computers to:

access an image sequence comprising a plurality of vascular images, the vascular images depicting a portion of a heart from a particular viewpoint and the vascular images being associated with different times within a time range;

30

determine a subset of the vascular images which are associated with a particular cardiac phase, wherein determining comprises computing a forward pass through a machine learning model trained to classify vascular images based on cardiac phase;

generate segmentation masks associated with the subset, wherein the segmentation masks segment vessels included in the respective vascular images which form the subset, wherein mask scores are determined for the segmentation masks which are indicative of a size or length associated with a vessel included in a segmentation mask, and wherein the subset is filtered to remove one or more vascular images based on the mask scores; and

determine a particular vascular image included in the filtered subset, wherein the determination is based on analyzing one or more image quality measures determined for each vascular image included in the filtered subset,

wherein the particular vascular image is configured for inclusion in an interactive user interface.

18. The computer storage media of claim 17, wherein to determine a subset of cardiac phase images, the instructions cause the one or more computers to:

determine whether the image sequence is associated with a left-side or a right-side of the heart,

wherein the machine learning model is selected from a plurality of machine learning models based on the determination.

19. The computer storage media of claim 17, wherein the image sequence is determined to be associated with a left-side or a right-side of the heart,

wherein for the right-side, a single segmentation mask is generated for each vascular image included in the subset, or

wherein for the left-side, two or more segmentation masks are generated for each vascular image included in the subset.

20. The computer storage media of claim 17, wherein to determine a particular vascular image, the instructions cause the one or more computers to:

register the vascular images included in the filtered subset, wherein registering comprises aligning features depicted in the vascular images;

determine image quality measures comprising contrast scores for the vascular images included in the filtered subset, wherein a contrast score indicates an average grayscale value associated with vessels in the vascular images; and

determine the particular vascular image based on the contrast scores.

* * * * *